ELSEVIER

Contents lists available at ScienceDirect

Cement and Concrete Research

journal homepage: www.elsevier.com/locate/cemconres



Effect of metakaolin and fly ash on the early hydration and pore structure of Portland cement

Vanda Papp ^{a,b}, Ioan Ardelean ^c, Anna Bulátkó ^d, Krisztina László ^d, Attila Csík ^e, Róbert Janovics ^b, Mónika Kéri ^{a,*} [©]

- ^a University of Debrecen, Department of Physical Chemistry, Egyetem tér 1, Debrecen H-4032, Hungary
- b Isotoptech Zrt., Debrecen H-4026, Hungary
- ^c Technical University of Cluj-Napoca, Department of Physics and Chemistry, 400114 Cluj-Napoca, Romania
- d Department of Physical Chemistry and Materials Science, Faculty of Chemical Technology and Biotechnology, Budapest University of Technology and Economics, H-1521, Budapest, PO Box 91, Hungary
- e HUN-REN Institute for Nuclear Research, H-4026, Debrecen, Bem tér 18/C, Hungary

ARTICLE INFO

Keywords: Cement Pozzolans Hydration Pore structure Permeability NMR

ABSTRACT

Substituting cement with pozzolans is important for various applications, like radioactive waste management. In this study, 10–30 % metakaolin and fly ash were added to Portland cement to gain insight into their effects on the structure formation, pore structure, and surface properties of cement. Early hydration of these composites was monitored using NMR relaxometry, showing that metakaolin exhibited pozzolanic activity after 8 h, while filler effect was observed for fly ash. FFC NMR and T_1 - T_2 correlation relaxometry revealed stronger water-solid interaction for the composites compared to pure cement. The dominance of the CSH gel pores increased with the additives in dry and wet state. Water diffusion in the capillary pores, followed by H_2 O- D_2 O exchange, was slower in metakaolin composites than in fly ash containing samples. The novel combination of NMR, SEM and N_2 porosimetry showed an advantage of metakaolin additive over fly ash for the long-term safe disposal of radioactive waste.

1. Introduction

Cement has been part of human life for centuries, serving a broad range of purposes. One of its significant applications supports radioactive waste management, where it acts as a physical barrier and a base material for the solidification and stabilization of radioactive waste [1–3]. Low- and intermediate-level radioactive waste (LLW and ILW) is usually conditioned by cementation, the primary material of which is Portland cement [1–3]. It consists of several clinker phases: tricalcium silicate (C₃S), dicalcium silicate (C₂S), tricalcium aluminate (C₃A), tetracalcium aluminoferrite (C₄AF) and gypsum [4,5]. These inorganic crystalline materials transform into hydration products during chemical reactions with water (hydration). The major hydration phases are the crystalline portlandite (20–25 %, Ca(OH)₂) and amorphous calcium silicate hydrate (50–70 %, CSH, 1.7CaO·SiO_{2·}xH₂O). In addition to these, aluminoferrite trisulfate [Ca₂(Al,Fe)(OH)₆·12H₂O]X₃·H₂O, aluminoferrite monosulfate [Ca₂(Al,Fe)(OH)₆]X·H₂O (X = sulfate),

hydrogarnet (3CaO·Al $_2$ O $_3$ ·6H $_2$ O) and hydrotalcite (Mg₆Al $_2$ (CO $_3$)· (OH) $_1$ 6·4(H $_2$ O) are formed as minor phases [4,5].

The precipitation of the hydration products results in the formation of a heterogeneous porous solid structure, where the main hydration product, the CSH gel determines the mesostructure of the cement. There are several models describing the structure of the CSH gel, among which the most accepted ones are the continuous model by Feldman and Sereda, and the colloidal model by Jennings [6,7]. The continuous model describes the CSH gel as a disordered, continuous assembly of highly defective CSH sheets [6,8–12], and distinguishes four pore types with different sizes: intra CSH sheet pores (d=0.5-1.8 nm), inter CSH gel pores (d=2-10 nm), capillary pores (d=20/50 nm–600 nm) and air pores (d=20/50 nm size) [9,13].

The hydration products have two important roles from the point of view of radioactive waste conditioning: they can bind radionuclides as sorbents and can affect the diffusion of water and radionuclides as a solid matrix [5,14]. The hydrated phases of the hardened cement

E-mail addresses: papp.vanda@science.unideb.hu (V. Papp), ioan.ardelean@phys.utcluj.ro (I. Ardelean), bulatko.anna@edu.bme.hu (A. Bulátkó), laszlo. krisztina@vbk.bme.hu (K. László), csik.attila@atomki.hu (A. Csík), janovicsrobert@isotoptech.hu (R. Janovics), keri.monika@science.unideb.hu (M. Kéri).

 $^{^{\}star}$ Corresponding author.

provide many options for the sorption of radionuclides present in dissolved form, including surface/ bulk sorption, incorporation or solid solution formation and precipitation [2,5]. The CSH gel has the highest sorption capacity due to its large specific surface area (\sim 148 m²/g), which enables the binding of both cations and anions depending on the Ca/Si ratio of the gel [5]. Crystalline portlandite has lower sorption ability, but can strongly sorb metal ions, like Ni, and halogens due to its layered structure and the numerous OH functional groups on its surface [5]. The minor hydration phases facilitate the ion exchange/ substitution or incorporation of the radionuclides [5].

In terms of radioactive waste conditioning, it is important to improve the sorption properties of the binders, which can be achieved by different additives (e.g. artificial silicates) [1]. Of course, these additives can significantly influence the mineral composition and thereby the pore structure, i.e. the size and the ratio of the pores, of cement. Degefa et al. showed the effect of metakaolin and fly ash on the mineral composition of cement using machine learning (ML) algorithms [15]. Both materials have high Si/ Al content and can participate in the hydration processes of Portland cement through pozzolanic reactions [16-19]. It was found that the additives increased the contribution of the CSH gel and the aluminum-containing minor phases (aluminoferrite monosulfate, hydrogarnet, hydrotalcite) in the hardened cement, while that of the portlandite and ettringite decreased [15]. Metakaolin increases mainly the ratio of CSH gel, while fly ash increases the ratio of aluminumcontaining phases [15] The use of additives is favorable for radioactive waste management, since among other benefits, they can increase the amount of sorbing phases and decrease the permeability of the binder. These properties are significantly related to the pore structure of the materials, which can be well studied with the classical characterization techniques (e.g. N2 porosimetry, SEM) as well as with less common liquid- phase NMR (Nuclear Magnetic Resonance) methods [10,11,17,20-23]. The advantage of the latter ones is the detection of the water content of cement which enables the characterization of water mobility and the wet structure. Through the transverse (T_2) and longitudinal (T_1) relaxation rates of protons in the hydrated cement structure, water domains of different mobility can be distinguished, and related to the pores and components of cement [24,25]. By NMR relaxometry the hydration process of cementitious materials and the evolution of the pore system can be followed and also the effect of various additives can be easily revealed [11,22,23,26-29]. The knowledge about the early hydration of cements can be further detailed with the frequencydependent measurement of the T_1 relaxation rate, informing about the surface evolution and the dynamics of the confined water molecules during the hardening process [11]. The joint use of these relaxation techniques provides multifold information about the early pore and surface formation process, which is essential for assessing the behavior of the binder during the radioactive waste conditioning and also for some practical aspects (e.g. rate of solidification). From the point of view of the long-term waste management, the leachability and permeability of the hardened cement is a key point, which can be gained from NMR diffusion measurements. Using the so-called H₂O-D₂O exchange diffusion technique the diffusion coefficients of water in the pore structure of cements can be obtained, while two-dimensional T_1 - T_2 correlation NMR experiments shed light on the exchange processes of water molecules between the different pore types [20,22,30].

On this basis, the aim of this study was to describe in detail the effect of two pozzolans (metakaolin and fly ash) and their concentration on the early hydration, structure formation and hardened pore structure of Portland cement, using the novel combination of the above-mentioned NMR methods, SEM and N_2 porosimetry. The applied water-solid and additive ratios might be suitable for the present radioactive waste management requirements [31]. The early hydration of pozzolan containing cement composite samples was followed by low-field NMR relaxometry techniques. The porous structure of the hardened composites was characterized by scanning electron microscopic imagining (SEM) and N_2 porosimetry in dry state and by several liquid-phase NMR

methods in wet state. 2D T_1 - T_2 correlation NMR relaxometry and H_2O - D_2O exchange diffusion measurements were carried out to gain information about the permeability of the porous structure. The overall goal was to thoroughly describe how the two studied pozzolans influence the pore structure of the composites and their interaction with water, which has a key role in the long-term safe disposal of radioactive waste.

2. Materials and methods

2.1. Preparation of cement samples

Two sample series were prepared using Portland cement (Duna-Dráva Cement Ltd., CEM I 42.5 N, 5–30 $\mu m)$ mixed with metakaolin (Keramost Plc., KM60, $d_{92} < 63 \mu m$) and fly ash (NEWCHEM GmbH, Microsit®10, $d_{95}\sim10~\mu m)$ separately in 0, 10, 20 and 30 m/m% mass ratio (detailed in Table 1.). Metakaolin consisted of 50-55 % SiO₂, min. $40~\%~Al_2O_3,\,max.~1.45~\%~Fe_2O_3,\,0.05-0.5~\%~CaO,\,0.20-0.45~\%~MgO$ and max. 1.5 % $K_2O + Na_2O$. The fly ash was a PFA type anthracite ash (class F fly ash) with a composition of 52 % SiO₂, 25 % Al₂O₃, 7 % Fe₂O₃, 5 % CaO. The dry powders were mixed with distilled water in 0.5 water-solid (w/s) ratio, motivated by the fact that at this ratio the hydration process can be considered complete, and the resulted cement paste has good workability, but still low permeability, which all are suggested features in the present radioactive waste management practice [1,31,32]. The pastes were poured into 2×0.6 cm cylindrical molds and cured for 30 days at 100 % RH. To follow the hydration process of the cement composites, the samples were prepared as detailed above, in-situ before the measurements.

2.2. Scanning electron microscopic imagining (SEM)

The surface morphology of the modified cement samples was investigated with a dual beam scanning electron microscope type Thermo Fisher Scientific-Scios 2 (FIB-SEM, Waltham, MA, USA), equipped with Bruker Quantax Energy Dispersive X-ray system (EDS) for composition analysis. The samples were crashed into several hundred micrometer pieces, homogenized and mounted on an aluminum sample holder before microscopic examination. A small amount of each sample was placed on conductive double-sided carbon adhesive tape, fixed on an aluminum holder and placed in the vacuum chamber of the microscope for further examination. To avoid the charge accumulation, the microscope was operated at fairly low accelerating voltage (5 keV) and current (0.1 nA). Since the penetration depth of accelerated electrons decreases with decreasing energy, this results in a decrease in the volume of the interaction. At low accelerating voltage the excitation volume shrinks in the specimen and the secondary electrons generated near the surface can easily escape, which increases the secondary electron yield. The higher yield increases the probability of collecting the electrons needed for imaging, thereby providing the opportunity to examine insulating samples. Applying such low energy allows us to study surface morphology of insulating samples without coating them with gold layer, which may modify the surface morphology.

Table 1Composition and name of the prepared cement composites.

| | Cement | Mc10 | Mc20 | Mc30 | Fc10 | Fc20 | Fc30 |
|---|--------|------|------|----------|------|------|------|
| Portland cement (m/m%) Metakaolin (m/m %) | 100 | 90 | 80 | 70 | 90 | 80 | 70 |
| | - | 10 | 20 | 30 | - | - | - |
| Fly ash (m/m%) Water/solid ratio | - | - | - | - 0.5 | 10 | 20 | 30 |

2.3. Low temperature nitrogen adsorption

Low temperature ($-196\,^{\circ}$ C) nitrogen adsorption isotherms were measured by a NOVA 2000 (Quantachrome) automatic analyser. The cement samples (pure Portland cement, 10–30 % metakaolin and 10–30 % fly ash containing cement) were evacuated at $110\,^{\circ}$ C for 24 h before the measurement. The apparent surface area S_{BET} was calculated using the Brunauer–Emmett–Teller (BET) model [33]. The pore volume ($V_{0.95}$) was estimated from the amount of nitrogen adsorbed at relative pressure 0.95, assuming that the pores are then filled with liquid adsorbate. The micropore volume (V_{micro}) was derived from the Dubinin–Radushkevich (DR) plot [34]. As no kernel files are available for cements, the pore size distribution in the mesopore range was also calculated from the Barrett, Joyner and Halenda (BJH) model from the adsorption branch of the isotherms [35]. Transformation of all the primary adsorption data was performed by the Quantachrome software ASiQwin version 3.0.

2.4. NMR relaxometry

The curing process of cement composites was followed by NMR relaxometry for which Portland cement was mixed with metakaolin and fly ash according to Table 1. The cement pastes were immediately poured into an NMR tube (10 mm), and the T_2 relaxation decays were recorded on a 20 MHz NMR instrument (Minispec mq20, Bruker, Germany) at room temperature (25 °C) using the CPMG (Carr-Purcell-Meiboom-Gill) pulse sequence for 48 h [36]. The echo time and the relaxation delay were 0.08 ms and 5 s, respectively. The obtained exponential curves were inverse Laplace transformed in the MERA (Multi Exponential Relaxation Analysis) program running under Matlab software [37]. This data evaluation method results in a T_2 distribution with the most characteristic relaxation times in the maxima. These values were further confirmed by multi-exponential fitting based on the least squares' method with the OriginPro \odot program.

For the pore structure characterization experiments the hardened cylindrical samples were soaked in deionized water (MilliQ) for several days and vacuum was used to remove the remaining air from the samples and to fully saturate the porous structure. Then the samples were removed from the water and the remaining water droplets were wiped off from the surface of the samples, to detect only the water in the pore structure. The cement samples were placed into 10 mm glass NMR tubes, and the T_2 relaxation decay was measured and evaluated as described above.

For the T_1 - T_2 NMR correlation relaxometry measurements three hardened cylindrical cement samples were selected: the pure Portland cement, the Mc20 and Fc20 composites. The samples were soaked in deionized water (MilliQ) and prepared the same way as for the NMR relaxometry measurements. During the 2D NMR relaxometry experiment, the transverse (T_2) relaxation times are measured simultaneously, encoded into the longitudinal (T_1) relaxation measurement. For this, the IR (inversion-recovery) pulse sequence is modified with the CPMG sequence, where after the 180° inverting pulse and a variable delay (t_1) CPMG measurements are carried out, the first data points of which result in the data points of the T_1 relaxation decay [10]. This way a twodimensional experimental data set is obtained, that contains information about the correlation of the relaxation times. The two-dimensional Laplace inversion of this data matrix results in a T_1 – T_2 correlation map. The total correlation measurement was carried out in two steps: first to follow the fast-relaxing components the delay time (t_1) in the T_1 measurement varied between 0.05 ms and 50 ms, with an increment of 0.1 ms, then to follow the whole relaxation process, t_1 was increased in 10 ms steps between 0.05 ms and 1000 ms. The two data matrixes were merged. The parameters of the CPMG measurement were set similarly to 1D NMR relaxometry. For the evaluation of the 2D data matrix a MATLAB® script package, the Upen2DTool program was used [38].

2.5. Fast field cycling NMR relaxometry

The frequency dependence of the longitudinal relaxation (T_1) time over the early hydration process of pure Portland cement, 20 % metakaolin and 20 % fly ash containing cement pastes were measured. The first 5 h of the cement hydration (*I-III. periods*) were followed at eight steps.

The measurements were performed with the fast field cycling technique using a FFC instrument (SMARtracer, Stelar SRL, Italy), which allowed the polarization and detection of the nuclear spins at higher fields while relaxation can take place at lower fields [8,11,39]. This measuring concept significantly increases the sensitivity of detection. The longitudinal relaxation (T_1) measurements were carried out at different Larmor frequencies (10 kHz-10 MHz). One measure consists of three steps: first the sample is polarized in a higher field B_p for a duration t_p until it reaches saturation. Then the magnetic field is switched to a lower field (B_r) , where the nuclear spins relax over the relaxation time t_r . After that the field is switched to the higher detection field (B_d) , where the remaining relaxation of the spins are detected by a 90°RF pulse [8,11,39]. Here the applied switching time determines the detectability of the fast-relaxing compounds, and the lower limit of this value was 2 ms in our case. The samples were prepared in situ before the measurement just like for NMR relaxometry, and were kept at 25 °C. The resulting dispersion curves were evaluated with the 3TM software package provided by Kogon and Faux [40].

2.6. Diffusion experiments

The diffusion of water was studied in hardened cylindrical samples of 20-24 mm length and 6 mm diameter. The cylinders were soaked in distilled water for several days, then placed in at least tenfold ($\alpha = 10$) excess of heavy water (D2O, VWR) immediately before the measurement. The pD was previously adjusted to the pH of the soaking water (pD \sim 13), using cc. NaOD. The NMR measurement was performed on a 20 MHz NMR instrument (Minispec mq20, Bruker, Germany) at room temperature (25 °C). During the experiment, the intensity of water protons within the sample was recorded as a function of time by FID sequence, through 512 sans, to obtain a high signal to noise ratio. The relaxation delay was set to 0.5 s, thus only the change in the amount of water located inside the cement samples was detected, with a minimal contribution of the external liquid (~18 %). The exchange process between H₂O and D₂O was followed every 5 min for 7 days in case of pure cement and metakaolin containing composites and for 4 days in case of the fly ash containing ones. The resulting intensity values were plotted as a function of the observation time after correction and normalization.

3. Results and discussions

3.1. Effect of pozzolans on the structure formation and pore structure of Portland cement

3.1.1. NMR relaxometry

As the dry cement clinker phases come into contact with water, a series of complex chemical processes take place, which include the complete or partial dissolution of the clinker phases and the formation of new hydration products. Among the clinker phases, the tricalcium aluminate (C_3A) and tricalcium silicate (C_3S) phases are the most important in terms of cement hydration [41]. The process is mostly dominated by the main clinker phase C_3S , resulting in the precipitation of amorphous CSH gel and crystalline portlandite [4]. The hydration of C_3A , in the presence of sulfates (gypsum) leads to the precipitation of ettringite, which can further develop to monosulfoaluminate, when the sulfate depletion point is reached [4]. This monosulfoaluminate forms in parallel with the precipitation of the CSH gel. [4]

The formation of hydration products leads to a decrease in the size of the voids filled by water, thereby changing the confinement and mobility of water molecules [22]. This can be easily monitored by NMR relaxometry as the T_2 transverse relaxation time of water highly depends on the size of the confining space:

$$\frac{1}{T_2} = \xi \frac{S_p}{V_p} + \frac{1}{T_{2bulk}} \tag{1}$$

where ξ is the surface relaxivity, S_p is the surface and V_p is the volume of the pores [42]. Water types with different rotational correlation times (τ_c) can be distinguished based on the T_2 relaxation time constant, since it is sensitive to slow solvent motion $(1/T_2 \sim \tau_c)$ [43]. The quantitative contribution of the different water types can be specified by the amplitudes related to T_2 . A more detailed theory of the method is presented in the Supporting Information.

The early hydration of the six pozzolan containing cement samples (see Table 1) was followed by measuring the T_2 relaxation of water in time for two days. Fig. 1 shows the determined T_2 values (a, b) and corresponding amplitudes (c, d) over time in case of the 10 % metakaolin (Mc10) and fly ash (Fc10) containing cement samples. Four water domains with different "mobility" characterized the cement composites. The fourth water domain is not shown in Fig. 1, as its contribution was <1 % and the T_2 relaxation times (T_{2d} decreasing from 200 ms to 12 ms) related to this domain were uncertain during the early hydration. This domain probably belongs to the larger capillary pores [9,11,44]. The water domain with $T_{2c} = 9-1.5$ ms can be assigned to the water, which first fills the smaller capillary pores, and then transforms to inter CHS gel pores during the hydration process, as the hydration products (mainly CSH gel) precipitate. Water domains with shorter T_2 relaxation times (T_{2a} varies between 0.10 and 0.13 ms and T_{2b} decreases from \sim 2 ms to 0.5 ms) can be assigned to water filling the intra CSH sheet pores of different sizes, the amount (A_{a-b}) of which will increase, as the CSH gel

forms. Similarly to Fig. 1, the change of T_2 and A over the early hydration are shown in Fig. SI 1–3. for cement and all the six pozzolan containing composites.

Comparing the T_2 relaxation times in Mc10 and Fc10, Fig. 1. shows that the shortest relaxation times related to the intra CSH sheet pores do not differ essentially, while their amplitudes ($A_{a.b}$) are more dominant in the case of Fc10. The most significant change in the T_2 and the amplitude during the hydration occurs in the third water domain. The initial value of T_{2c} is shorter in case of Fc10 ($T_{2c} = 6.4$ ms), than for Mc10 ($T_{2c} = 8.9$ ms), and the decrease of this relaxation domain is prolonged for the fly ash containing sample.

The five well-known stages (I-V) of the hydration process are reflected by the observed T_2 relaxation times and are indicated in Fig. 1a and b with roman numbers. The initial dissolution (I) period is difficult to follow, since it lasts only for several minutes (<15 min) and is not shown [4]. In this period the fast dissolution of the most reactive clinker phase (C₃A) takes place resulting the precipitation of ettringite, which leads to the drastic decrease of the T_2 values due to a sudden decrease in the size of the space and the presence of dissolved magnetic impurities [4,11,22,23]. Also, the dissolution of C₄AF occurs, resulting in increasing paramagnetic ion concentration. Thereafter, in the induction (II) period, the T_2 relaxation times stagnate as can be seen on Fig. 1a, b. There are several theories to explain this phenomenon, among which the dissolution control and protective membrane models are the most widespread [45,46]. According to the previous one, a supersaturated calcium and silicate solution is required for the formation of portlandite, which subsequently drives the precipitation of CSH [11,45,46]. In contrast, the protective membrane theory assumes the formation of a coating layer on the cement grains, hindering the exchange between gel and bulk water, prolonging the supersaturation [45,46]. During this period, no notable structural changes take place that would alter the T_2

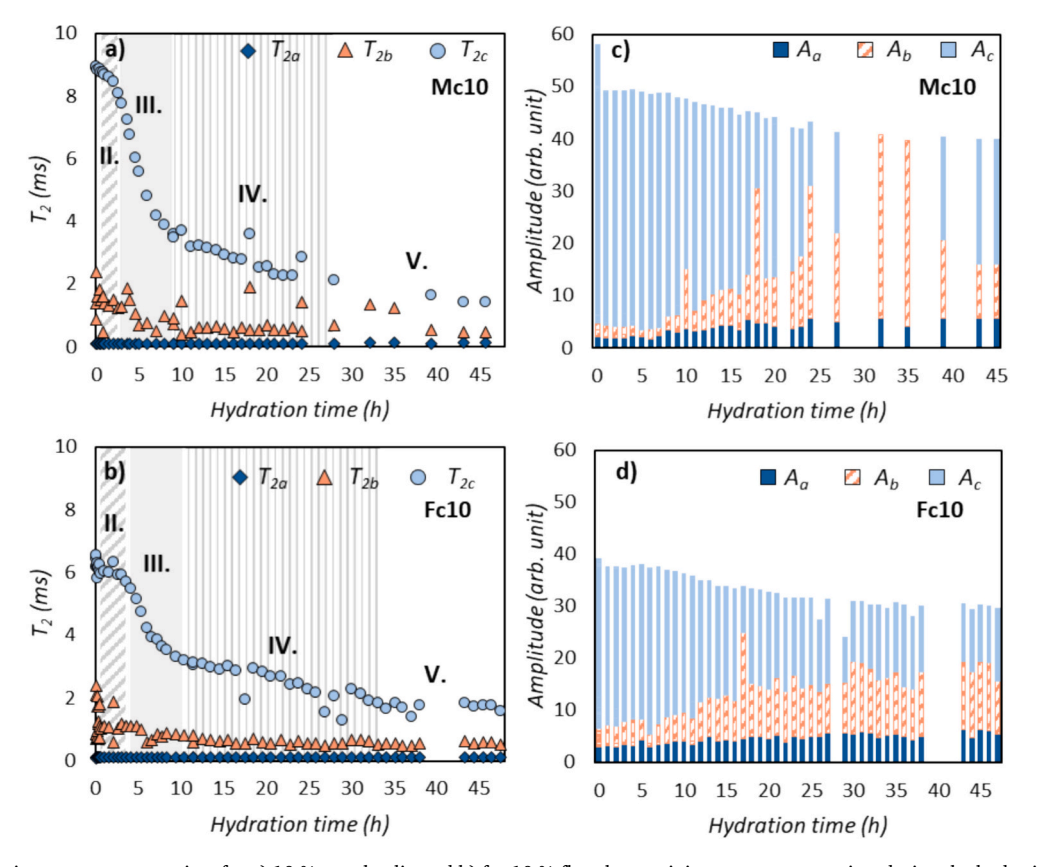


Fig. 1. T_2 relaxation time constants over time for a) 10 % metakaolin and b) for 10 % fly ash containing cement composites during the hydration process. Different colors show water in the intra CSH sheet (T_{2a} , dark blue, diamond), inter CSH gel (T_{2b} , orange, triangle) and smaller capillary pores (T_{2c} , light blue, circle). The different stages of the hydration process are indicated in Roman numerals and detailed in the text. c-d) The change of the amplitudes of the listed water domains, with the same colour. (For interpretation of the references to colour in this figure legend, the reader is referred to the web version of this article.)

relaxation time. The acceleration period (*III*) occurs as the critical concentration of calcium and silicate is reached and the massive precipitation of CSH and portlandite begins, resulting in the sharp decrease of T_2 as the size of the confining space decreases. The transformation of ettringite into monosulfate takes place parallelly [4]. During this time, the amplitudes of the most bound water types (A_{a-b}) significantly increase as the hydration products fill out larger confinements and form the nanoscale structure of the binder. In the deceleration (IV) and slow hydration periods (V), the decrease of T_2 slows down, as the rate of the precipitation of CSH decreases due to the hindered diffusion of water within the densifying system. The total amplitude of the water in the system also decreases during the hydration process, since water takes part in the hydration reactions (Fig. 1c, d).

In the presence of pozzolans, the hydration process is slightly more nuanced, as the additive containing active silicate and aluminate can also participate in hydration reactions [23,47,48]. According to several studies, the pozzolanic effect plays a significant role only in the later stages of hydration, and during the early hydration, additives are considered as chemically inert fillers [23,47,49,50]. Due to the presence of pozzolans in the solidified samples, the additional alumina and silica introduced by the additive are partially incorporated into the CSH gel, leading to the formation of CASH (calcium-alumino-silicate hydrate) gel alongside the CSH gel. The pozzolans also enhance the formation of aluminate-containing hydration products (such as monosulfoaluminate, hydrogarnet, hydrotalcite), while decreasing the quantity of portlandite [15].

To draw more profound conclusions about the effect of pozzolans on the hydration of Portland cement, the amplitude weighted T_2 relaxation times $(\overline{T_2})$ were calculated based on [51]:

$$\overline{T_2} = \frac{\sum_a^i A_i \times T_{2i}}{\sum_a^i A_i}$$

where A_i is the amplitude, T_{2i} is the transverse relaxation time constant of the i-th water domain (i=a-d) at t hydration time. $\overline{T_2}$ better emphasizes the changes in the system during hydration as it smooths the uncertainty resulting from the Laplace inversion. Fig. 2 shows the decrease of $\overline{T_2}$ over the early hydration of the cement composites, which mainly reflects the change of T_{2c} .

We studied the hardening process of pure Portland cement previously and for the interpretation of the effect of pozzolans, these results were used for comparison (see on Fig. 2a) [22].

The first noticeable difference between the two pozzolans is the initial value of $\overline{T_2}$. Water relaxes significantly faster in case of the fly ash containing samples ($\overline{T_2} \sim 2.2$ –5.2 ms) compared to pure Portland cement ($\overline{T_2} \sim 7.4$ ms) and the metakaolin incorporated composites ($\overline{T_2} \sim 8.2$ ms). This difference can be explained by two effects according to Eq. 1: the size of the confinements is smaller in the fly ash composites or the surface properties of the solid (surface relaxivity – ξ) differ. The latter one depends significantly on the iron content of the additive, that causes higher magnetic inhomogeneity because of the paramagnetic moment of Fe³⁺. According to the composition of the additives, the iron content of fly ash is higher compared to metakaolin (see in Section 2.1).

The second clearly visible difference between the pozzolans is the way they affect the hydration process, the length and the speed of the above detailed periods. Metakaolin mainly exerts its influence on the deceleration (*IV*) period, where the CSH gel and monosulfoaluminate precipitation occurs at a moderate rate. Higher metakaolin

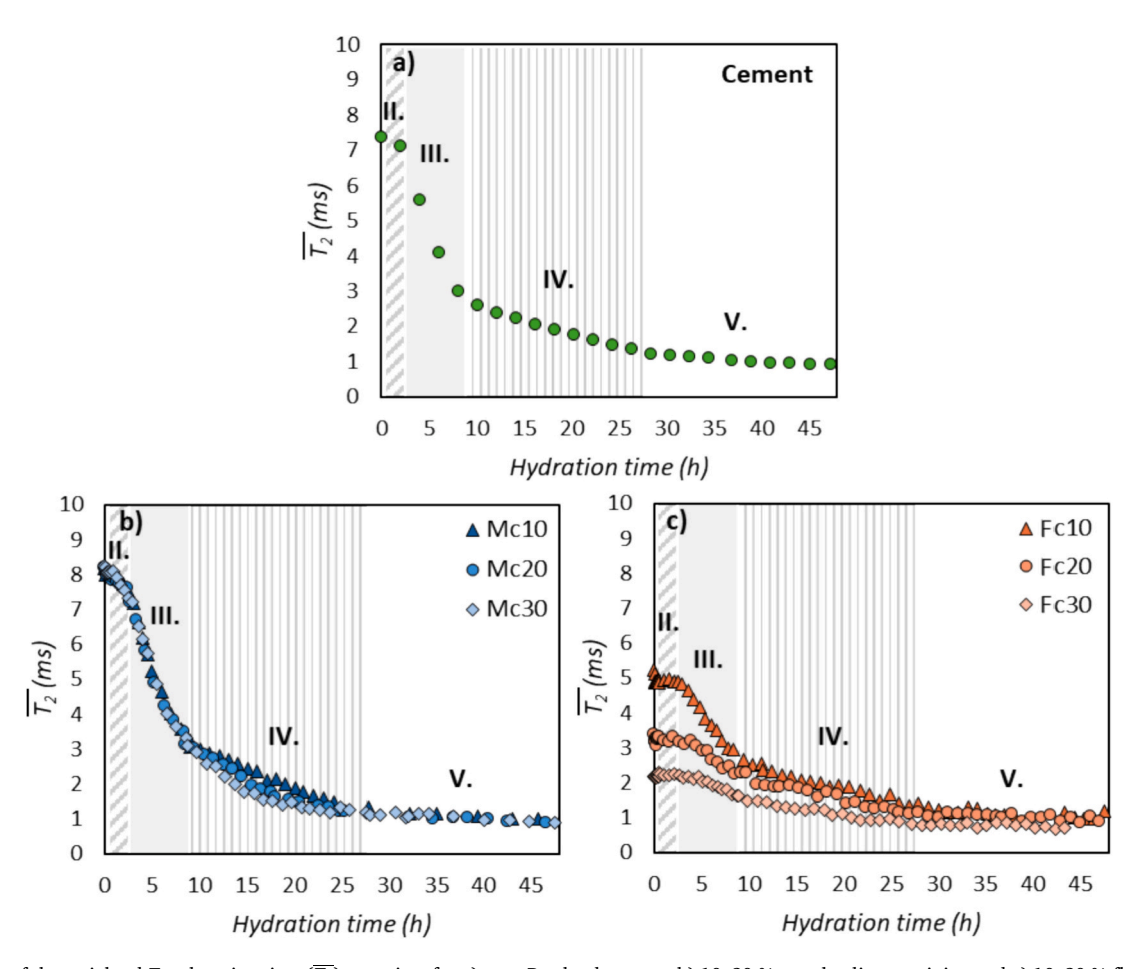


Fig. 2. Change of the weighted T_2 relaxation time ($\overline{T_2}$) over time for a) pure Portland cement, b) 10–30 % metakaolin containing and c) 10–30 % fly ash containing cement composites during the hydration process. The different stages of the hydration process are indicated according to the pure Portland cement for comparison.

concentration increases the rate of the deceleration period, thus the speed of precipitation (slope of the curve). The length and the course of the other periods are similar to those of pure cement. In contrast, fly ash highly affects the whole hydration process: the duration of the induction period (II) prolonged, the speed of the acceleration (III) and deceleration (IV) periods decreased. These effects become more dominant with increased amount of the additive. The differences between metakaolin and fly ash can be explained by the higher pozzolanic activity of metakaolin [50]. Metakaolin, as a synthetic aluminosilicate, is able to take part in the initial periods of the cement hydration process due to its higher active aluminate and silicate content [18,19,49]. Aluminate and silicate easily release from the amorphous particles and can participate in the formation of additional CSH gel and other aluminum containing minor phases in the presence of portlandite (Ca(OH)2), resulting in faster precipitation [19,52]. This process, being responsible for the catalyzing effect of metakaolin on the cement hydration in the early stages, was also confirmed by higher cumulative heat evolution revealed in several isothermal calorimetry studies [53,54].

Fly ash can also react the same way as metakaolin, however during the early hydration it mainly acts as an inert filler material [18,23]. This additive is an industrial byproduct with higher impurity and inactive aluminate and silicate content, which pozzolanic activity in the early hydration is lower compared to metakaolin. [18,19,49] The differences in the hydration process of fly ash containing samples can be explained by the dilution or filler effect. This means that the spherical fly ash particles can adsorb the dissolved ions (e.g. Ca²⁺) and as inert fillers cause the increase in the apparent water-cement ratio (by replacing cement), which hinders the supersaturation of the pore solution and slows down the precipitation of the hydration products [19,23,48]. According to Skibsted and Snellings the available porosity of cement may also influence the pozzolanic reaction beyond the water availability [50]. Since metakaolin exerts its pozzolanic effect on cement hydration earlier than fly ash, simultaneously to the C3S cement phase, these limiting factors may have a smaller role compared to fly ash, where the growth of hydrates inside the refining pores may be more restrained (sustaining hydration needs larger driving force) [50].

3.1.2. FFC- NMR

To gain information on the surface evolution and the dynamics of the confined water molecules during the early hydration, FFC NMR measurements were performed [11]. The frequency dependent T_1 (longitudinal) relaxation of the confined water was measured during the first 5 h (I-III. periods) of the hydration process in the case of Portland cement, 20 % metakaolin and 20 % fly ash containing samples. Compared to the CPMG measurements, being sensitive to the presence of several types of bound water, the FFC measurements give an average T_1 value which is dominated by water in the capillary pores, as shown by the distribution of the water domains in Fig. 1. c-d [8,11]. The relaxation dispersion curves of the three samples over the first 5 h of the hydration are shown in Fig. 3. Similar features of the dispersion curves have already been observed in the case of gray cement samples [8,13,55,56]. The different pozzolanic activity of the additives is clearly visible on the evolution of the dispersion curves over time. A faster evolution occurs in the case of the 20 % metakaolin containing sample compared to the pure Portland cement paste, while the 20 % fly ash containing sample shows a slower evolution.

Since the T_I relaxation process is measured at several Larmor frequencies (0.01–10 MHz), it is sensitive to a wider range of molecular mobilities compared to a single frequency [11]. The resulting dispersion curves can be explained on the basis of the theoretical 3-Tau model proposed by Faux et al. [40,57,58] According to this model, the longitudinal relaxation process of confined water molecules within a porous system containing paramagnetic impurities (e.g. Fe^{3+}) is highly dominated by thermally modulated dipolar interactions between the proton spins and the spin of the unpaired electron of Fe^{3+} within the solid phase [11,40,57,58]. Based on the model, water is present within the porous solid structure in a bulk-like state and in a surface layer with the thickness of one water molecule ($\delta = 0.27$ nm) [11,40,57]. Water can

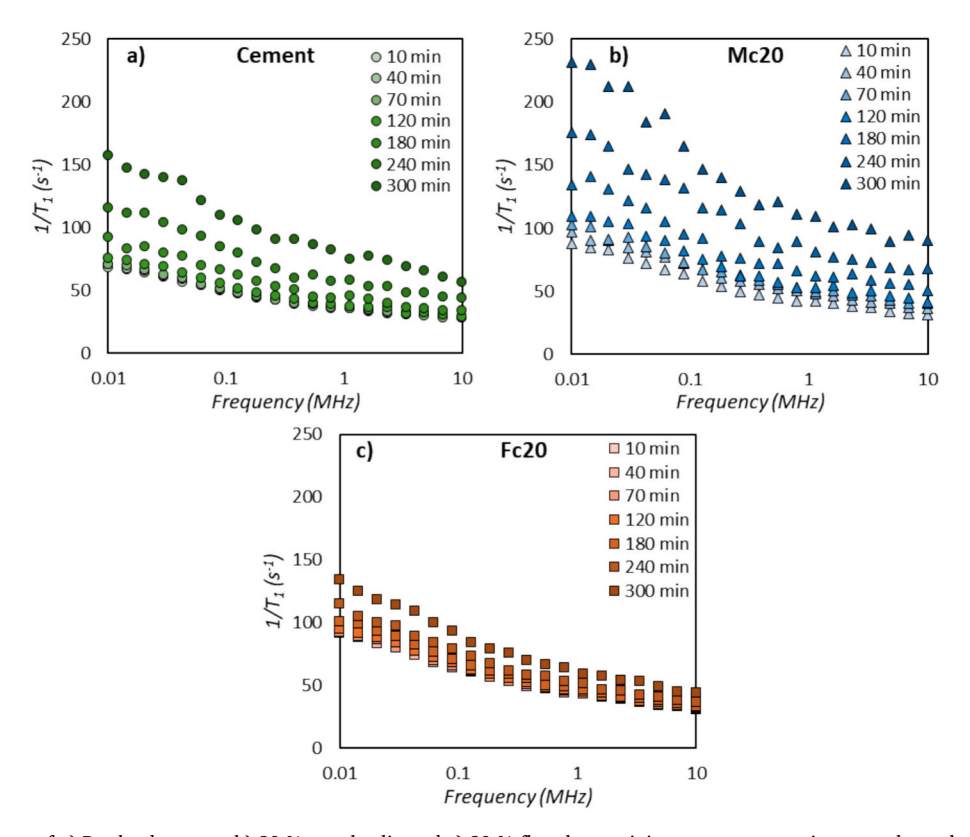


Fig. 3. T_I dispersion curves of a) Portland cement, b) 20 % metakaolin and c) 20 % fly ash containing cement composites over the early hydration process. From bottom to top, the dispersion curves are shown as the hydration progressed.

move in these environments; it can diffuse in the bulk phase and parallel to the surface in the surface water layer with characteristic diffusion time constants defined by the bulk and surface water diffusion coefficients: $D_{b,l} = \delta^2/_{6\tau_{b,l}}$ where D_b or D_l is the diffusion coefficient of water in the bulk (b) or in the surface layer (l), δ is the thickness of a "layer" of water and τ_b or τ_l is the diffusion correlation time constant of water in the bulk or in the surface layer [11,40,57,58]. The third type of water movement considered in the model is determined by the adsorption-desorption process of water molecules on the surface. This can be described by the desorption time (τ_d) which gives the time the molecules spend on the surface before desorption under the assumption

that the surface spins desorb as $exp\left(-t_{/\tau_d}\right)$ [11,40,57,58]. τ_d is longer,

when the interaction between the solid surface and the water molecules is stronger [11]. These displacements of water molecules within the porous structure can modulate the dipolar interaction between the nuclear spins of water and the electronic spins of the paramagnetic ions (Fe³⁺) [11,40,57,58]. Consequently, these three time constants (3-Tau: τ_b , τ_b , τ_d) will greatly affect the longitudinal relaxation process (T_1):

$$\frac{1}{T_1(\omega)} = f\left(\tau_l, \tau_b, \tau_d, N_{para}, \frac{S\delta}{V}\right)$$
 (2)

where N_{para} is the number density of the paramagnetic ions in 2δ depth within the solid matrix and $S\delta/V$ is the ratio of the volume of the surface layer (S – surface area) and the pore volume (V) [11,40,57,58]. The latter one can be applied to calculate the size of the planar pores (h), as the model supposes this geometry [11]. A software package (3TM) provided by Kogon and Faux was used for the evaluation of the dispersion curves, and for the extraction of the above-mentioned parameters (τ_b – bulk diffusion correlation time, τ_l – surface diffusion correlation time, τ_d – desorption time, N_{para} – number density of the paramagnetic ions, $S\delta/V$ – surface layer volume to pore volume) [40]. The fitted curves are shown in Fig. SI 4–5.

After a few iterations we concluded that the value of the bulk diffusion correlation time can be kept constant $\tau_b = 23.7$ ps. Generally, this value for pure water is $\tau_b = 5.3$ ps, however the presence of dissolved ions in cement pastes and the possible appearance of a second hydration layer can prolong τ_b [11,40]. Further parameters of the model were extracted from the fittings for each stage of the cement hydration and are shown in Fig. 4–5.

The change of τ_d and τ_l over the cement hydration in the three cement samples (Fig. 4), shows that the addition of the pozzolans had a different effect on the change of time constants compared to cement. Both

 τ_d (from 5.62 µs to 0.67 µs) and τ_l (from 0.49 µs to 0.1 µs) quasi decreased in case of pure Portland cement. On the contrary, in the case of Mc20 and Fc20 samples τ_d and τ_l slightly increase or stagnate, as shown in Fig. 4. The reason for the stagnating τ_l values up to 180 min for Fc20 and 70 min for Mc20 is that τ_l is sensitive to the slope of the dispersion curves which do not change in these time ranges (Fig. 3b and c).

The dissimilarity can be explained by the difference in the emphasis of the dissolution and precipitation processes during the early hydration, as well as the difference in the reactive surface area and particle size of the solid [59]. The rate of the dissolution and precipitation highly depends on the area of the interface between the solid and the solution, and the concentration of the ions in the solution [59]. As the concentration of the solvated ions increases, the dissolution rate of the main clinker phase (C_3S) decreases [59]. When the concentration of Ca^{2+} ions in solution is high enough, the precipitation of portlandite begins, involving the formation of CSH gel [11,59]. The substitution of cement with pozzolans increases the amount of water available for cement hydration, as it is not a reaction partner for the pozzolan. This results in a decreasing dissolution rate, thus prolonging the precipitation of hydration products [59].

Moreover, both the dissolution of the anhydrous clinker phases and the precipitation of the hydration products involves the release of heat, which highly affects the temperature of the surface, thus the rate of desorption [59,60]. Based on this, the heat evolution during the early hydration of the cementitious materials significantly affects τ_d as well as τ_l [60]. Moghaddam et al. found that the addition of fly ash decreased the cumulative heat evolution during the cement hydration and by increasing the content of the additive the heat evolution decreased [17]. Similarly, Frías et al. found that the hydration heat decreased in case of fly ash blended mortars compared to 100 % Portland cement mortar due to cement substitution and the dilution effect, while the metakaolin blended mortars produced slight heat increase during the first hours of the hydration [16]. However, it should be considered that during the early hydration, beyond the heat evolution, the area and the quality of the solid surface also changes as a consequence of the chemical reactions. Further discussion of these complex processes is beyond the scope of this study.

In summary, the change in τ_d for pure cement can be interpreted as: the initial dissolution derived by the undersaturated solvent causes the lower initial value ($\tau_d=4.87~\mu s$), which slightly increases as the rate of dissolution decreases (see in Fig. 4a). After the concentration of Ca²⁺ ions reaches supersaturation the massive precipitation of CSH begins, involving notable heat evolution. This evokes a decrease in τ_d . Similar processes take place for Mc20 and Fc20 as well but with a time delay,

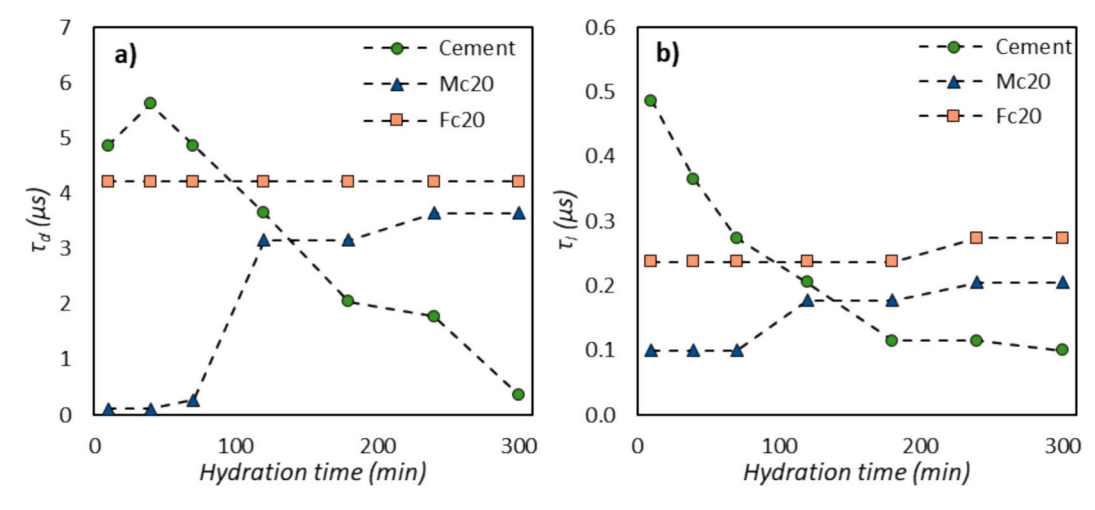


Fig. 4. The change of a) the desorption time (τ_d) and b) the surface diffusion correlation time (τ_l) of confined water over the early hydration of Portland cement (green circle), 20 % metakaolin (blue triangle) and 20 % fly ash (orange cube) containing cement samples. (For interpretation of the references to colour in this figure legend, the reader is referred to the web version of this article.)

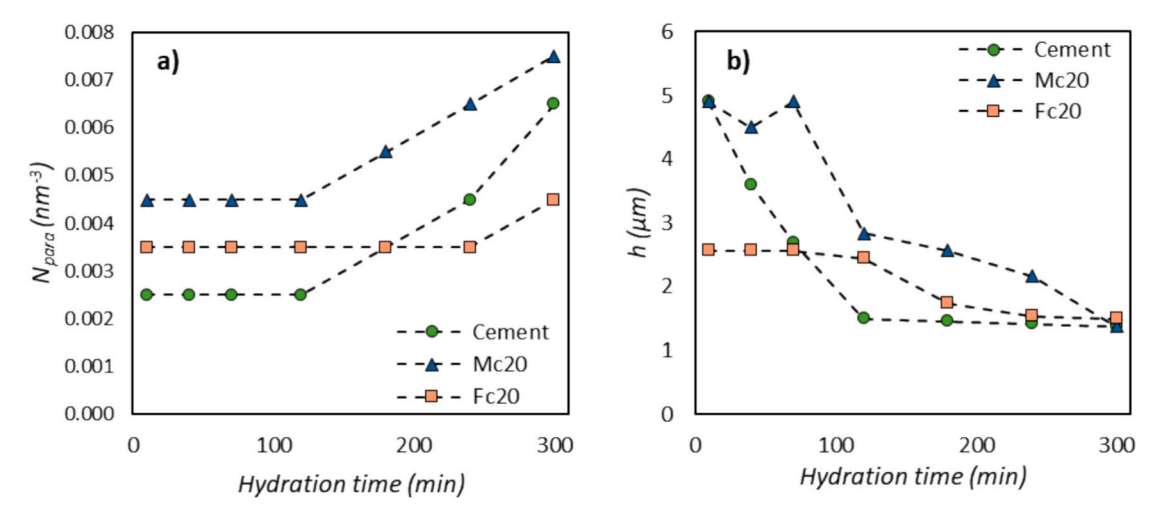


Fig. 5. The change of a) the number density of the paramagnetic ions (N_{para}) , and b) the size of the planar pores (h) during the early hydration. The samples investigated are indicated in the legend.

due to the filler effect. As the pozzolanic activity of metakaolin is higher compared to fly ash, τ_d starts to increase after 120 min as the dissolution slows down. The lower initial value of τ_d and τ_l compared to pure cement can be caused by the higher heat evolution during the hydration of the cement composite, that shortens the time water molecules stay adsorbed to the surface and in the surface layer. For Fc20, no change in τ_d and τ_l can be observed, the induction period is much longer for this additive as it was presented in Section 3.1.1.

To draw conclusions about the strength of the interaction between the water molecules and the surface, we compared the value of τ_d and τ_l at the end point of the measurement (t=300 min). In the case of both time constants, similar trend can be observed: water spent the longest time near the surface in Fc20 ($\tau_d=4.22~\mu s,~\tau_l=0.27~\mu s$), thus indicating a stronger interaction, while the interaction was the weakest for pure cement ($\tau_d=0.37~\mu s,~\tau_l=0.1~\mu s$).

The surface water diffusion coefficients (D_l), derived from the surface diffusion correlation times (τ_l), are shown in Table 2. The observable trend in time is the opposite of that of the τ_l and D_l values are identical where τ_l does not change (Fig. 4b). The determined coefficients are of the same order of magnitude as those found by Rusu et al., which was $D_l = 5.06 \times 10^{-14}$ m²/s [11]. The weakening interaction between water molecules and the surface of pure cement is also confirmed by the increase in diffusion coefficients in time.

The change in the number density of paramagnetic ions (N_{para}) in the three samples over the early hydration is shown in Fig. 5a. Two definite distinctions can be observed between the samples: i) the initial value of N_{para} and ii) the hydration time when N_{para} begins to increase, which can be explained by the processes in the induction period (II) of cement hydration, and the length of this stage. During this period a protective membrane/ layer of hydration products reduces the interaction between the bulk water and the surface of the cement grains. The thicker the layer, the weaker this interaction, and a smaller effective ion density is perceptible, according to Rusu et al. [11] In our case, the thickness of the protective layer is the lowest for the metakaolin containing sample

 $(N_{para}=4.5\times10^{-3}~{\rm spins/nm^3})$ and the highest for pure cement $(N_{para}=2.5\times10^{-3}~{\rm spins/nm^3})$. The value of N_{para} increases as the protective layer ruptures, and water can reach the solid grain as the acceleration period (III) begins [11]. The duration of the induction period (II) slightly elongates with the addition of fly ash, as it was discussed in Section 3.1.1.

The last parameters extracted from the fitting approach are the surface layer volume to pore volume ratio $(S\delta/V)$ and the derived size of the assumed planar pores (h), which dependence on the hydration time is shown in Fig. SI 6 and Fig. 5b, respectively. As the hydration products precipitate during the hydration process, the surface of the pores increases, while their size decreases. The filling of the micrometer-sized voids by hydration products is the fastest in the case of pure cement, followed by Mc20 and finally Fc20 in terms of speed due to their different pozzolanic activity. The h values at the beginning of the hydration are lower for Fc20, indicating the smaller available space for the precipitation of the hydration products as mentioned in Section 3.1.1.

3.2. Effect of pozzolans on the hardened pore structure of Portland cement

3.2.1. Dry state

During cement hydration various hydration products precipitate, which have two important effects from the point of view of radioactive waste conditioning: *i*) they can effectively sorb several radionuclides, and *ii*) their precipitation results in the formation of a heterogenous porous solid structure that affects the diffusion of water and radionuclides [5]. We investigated this porous structure and the structure-modifying effect of pozzolans in the case of the hardened cement samples in dry and aqueous environments.

The dry structure of the cement composite samples was studied and compared by N_2 gas porosimetry and scanning electron microscopic imagining (SEM). The SEM images of the pozzolan containing cement

Table 2Diffusion coefficients of water in the surface water layer over the early hydration of cement-based samples.

| $D_l (m^2/s)^a$ | | | | | | | |
|------------------------|---|--|--|--|--|--|--|
| t _h (min) b | 10 | 40 | 70 | 120 | 180 | 240 | 300 |
| Cement Mc20 Fc20 | $\begin{array}{c} 2.49 \times 10^{-14} \\ 1.22 \times 10^{-13} \\ 5.13 \times 10^{-14} \end{array}$ | $3.33 \times 10^{-14} \\ 1.22 \times 10^{-13} \\ 5.13 \times 10^{-14}$ | $4.43 \times 10^{-14} 1.22 \times 10^{-13} 5.13 \times 10^{-14}$ | 5.93×10^{-14} 6.83×10^{-14} 5.13×10^{-14} | $1.06 \times 10^{-13} \\ 6.83 \times 10^{-14} \\ 5.13 \times 10^{-14}$ | $1.06 \times 10^{-13} 5.93 \times 10^{-14} 4.43 \times 10^{-14}$ | $\begin{array}{c} 1.22{\times}10^{\text{-}13} \\ 5.93{\times}10^{\text{-}14} \\ 4.43{\times}10^{\text{-}14} \end{array}$ |

^a Surface diffusion coefficient.

^b Hydration time.

samples (Mc10–30 and Fc10–30) were taken on micrometer-sized pieces, which preserve the nanostructure according to our preliminary experiments, and are shown in Fig. 6 and Fig. SI 8, 9 in further magnifications. The SEM image of the applied pure Portland cement was previously published and used for comparison and for the interpretation of the pozzolan effect (Fig. SI 7) [22]. The degree of substitution of cement with pozzolans has great influence on the mineral composition of the hardened material: it can increase the amount of the calcium-silicate hydrate (CSH) and the aluminum containing minor phases, while decreases the amount of portlandite and ettringite, as detailed above [15,61].

Among these hydration products the spike-like calcium- silicate hydrate (CSH), the plate-like shaped portlandite (CH), and the needle-like ettringite (E) can be identified with great certainty in Fig. 6 and Fig. SI 8, 9. Their changes are observable on the images, as the amount of CSH visibly increases with the pozzolan content, while portlandite appears only at low concentration ($\sim\!10$ %). Ettringite is also visible in both samples, the contribution of which slightly decreases with increasing pozzolan content. In the case of fly ash containing samples, spherical, micro-sized fly ash particles (FA) can be identified, the surface of which is also coated with thin layers of hydration products. [61] Their size is between 1 and 6 μ m. The presence of these particles increases the heterogeneity of the samples as well as the macroscopic features of the pore structure.

In summary, the higher pozzolanic content of the composites increases the compactness of their structure, due to the excess hydration products formed in pozzolanic reactions. The highest compactness can

be observed at 20 % pozzolan content in the SEM images. The metakaolin containing composites showed a more contiguous solid matrix with less macroscopic voids compared to the Fc series.

The mesostructure of the dry hardened cement composites was studied by N_2 porosimetry as well, and the resulted N_2 sorption isotherms are shown in Fig. 7. The data deduced by the various models are summarized in Table 3. Due to the steep end of the isotherms the pore volume was estimated at $p/p_0=0.95$ ($V_{0.95}$). The sorption isotherms can be classified as IVa-II transition type with an H3 like hysteresis loop according to IUPAC [62]. This type of isotherm is characteristic for materials, where the pore structure is mainly composed of micro- and mesopores beside the macropores [62,63]. The hysteresis loop implies that the porous structure consists of non-rigid aggregates of plate-like particles (e.g., certain clays) or incompletely filled macropores of the pore network [62]. Increasing the pozzolan content moved the isotherms downward, indicating a decrease in the pore volume (Fig. 7).

All the micro-, meso- and "total" pore volumes (Table 3.) show a decrease with increasing metakaolin content compared to pure Portland cement. The microscale compactness observable in the SEM also holds for the nanoscale as reflected by the N_2 adsorption data. In case of fly ash composites, the micropore volume decreases, however the mesopore volume slightly increases with the fly ash content, causing an increment in $V_{0.95}$. The apparent surface area of the samples, S_{BET} , similarly to the micropore volumes, also decreases. The $V_{0.95}$ and the S_{BET} of the Fc composites are lower compared to the other samples. The explanation for these differences may lie in the dissimilar pozzolanic activity of the additives resulting in extra CSH gel formation to a various extent, the

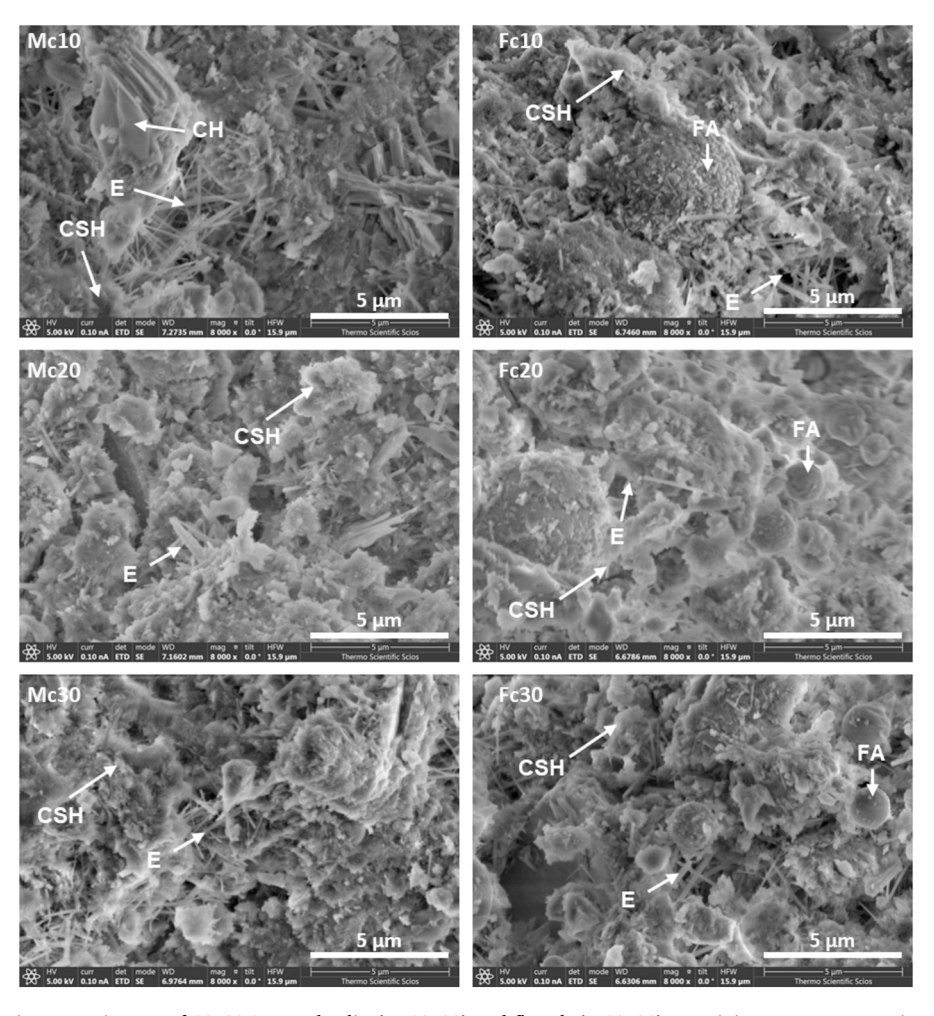


Fig. 6. Scanning electron microscopy images of 10–30 % metakaolin (Mc10–30) and fly ash (Fc10–30) containing cement composites showing the characteristic hydration products and the remaining pozzolanic additives. (CSH- calcium silicate hydrate, *E*- ettringite, CH- portlandite, FA- fly ash).

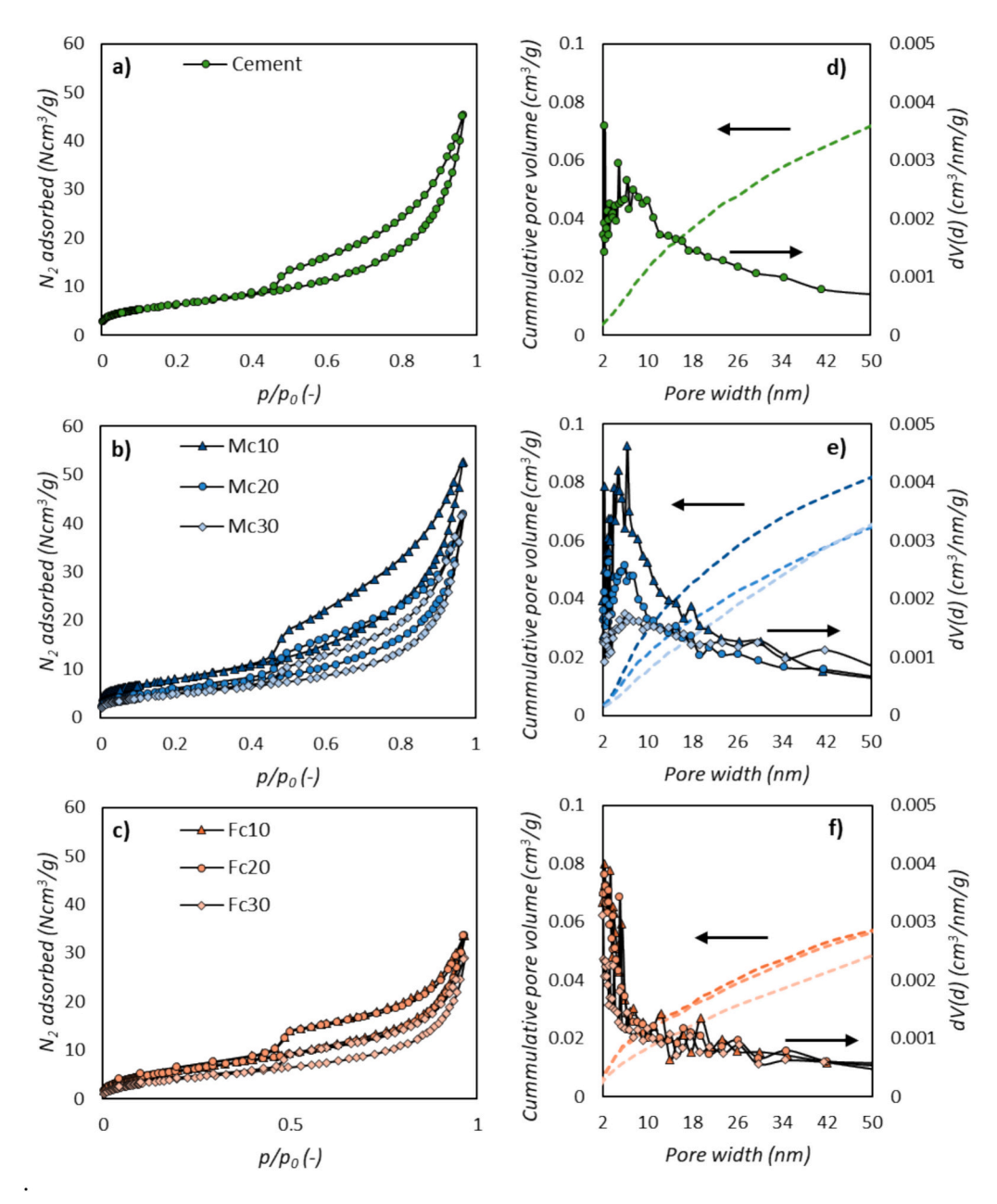


Fig. 7. Low temperature adsorption isotherms of the samples: a) Portland cement, b) 10–30 % metakaolin and c) fly ash containing cement composites. The derived cumulative pore volumes (left axis, dashed line) and pore size distributions (right axis, symbol and line) of d) Portland cement, 10–30 % e) metakaolin and f) fly ash containing cement composites.

Table 3Morphological properties of Portland cement and the pozzolan containing composites from nitrogen adsorption.

| Sample | $S_{BET} (m^2/g)^a$ | V _{micro} (cm ³ /g) b | $V_{0.95}$ (cm 3 /g) c | V_{meso} $(cm^3/g)^{d}$ | | |
|--------|---------------------|---|------------------------------|---------------------------|--|--|
| Cement | 23 | 0.0081 | 0.057 | 0.049 | | |
| Mc10 | 29 | 0.0108 | 0.068 | 0.057 | | |
| Mc20 | 21 | 0.0070 | 0.050 | 0.043 | | |
| Mc30 | 18 | 0.0061 | 0.049 | 0.043 | | |
| Fc10 | 23 | 0.0073 | 0.034 | 0.027 | | |
| Fc20 | 22 | 0.0072 | 0.042 | 0.035 | | |
| Fc30 | 16 | 0.0055 | 0.043 | 0.038 | | |

- ^a Surface area from BET model.
- ^b Micropore volume from DR plot.
- ^c Pore volume at $p/p_0 = 0.95$.
- ^d Mesopore volume $(V_{0.95} V_{micro})$.

micropores of which are partially filled with non-evaporable water and thus not accessible for nitrogen (further discussed in Section 3.3). According to the literature, hardened cement paste usually has a surface area $>50~\text{m}^2/\text{g}$ [5,64]. Our results are somewhat lower, which can be explained by the presence of porous regions separated by narrow entrances, or by the formation of closed pores due to the potential thermal damage of the hydration products, both being inaccessible for nitrogen [64,65].

The pore size distributions (shown in Fig. 7d-f) were obtained from the adsorption branch of the isotherm using the BJH model, which gives reliable results in the mesopore range, between 2 and 50 nm pore diameter. The maximum for Portland cement and the metakaolin containing samples is around 7 nm with a wide distribution over the examined size range. For the fly ash containing samples the maxima shifted to lower sizes (~ 2 nm), and the distribution became narrower, indicating the dominance of small mesopores and micropores.

3.2.2. Wet state

The knowledge of the pore structure and the behavior of cement composites in aqueous environment is essential since they ultimately affect the applicability of the binders in radionuclide waste management [1]. The effect of the additives on the hardened pore structure of cement in wet state, i.e. on the contribution of different pore types, on the permeability and on the diffusivity of confined water, was studied by various low- field NMR techniques.

The pore structure was described by the T_2 transverse relaxation of water confined in the heterogenous solid matrix. Since NMR detects the total proton intensity of the liquid in the samples, it provides information also on small, closed pores filled with water, which are not "visible" for other methods (e.g. N2 porosimetry, MIP). According to Eq.1 the relaxation of bound water in the smaller pores is faster (short T_2 relaxation time) than in larger pores, where the movement of water molecules is less hindered, in case of slow exchange between the two domains. Based on the dependence of T_2 relaxation time on the S/V ratio of the confinement, the identification of the typical pore types of cement is possible based on the resulted T_2 distribution curves as shown in Fig. 8a, b. Water domains with short T_2 relaxation times can be assigned to bound water in the smaller intra CSH layer pores ($T_2 < 1$ ms, marked with blue on Fig. 8a, b) [9,21,22]. The next relaxation time range, 1 ms $< T_2 < 5$ ms, can indicate slightly more mobile water in the inter CSH gel pores [9,21,22]. Water domains whose T_2 is longer than 5 ms were defined as water filling the capillary pores [9,21,22]. The applied limits were deduced from the relaxation times estimated according to the characteristic pore sizes.

Comparing the T_2 distribution curves of pure Portland cement (Fig. 8a) and the pozzolan containing composites (Fig. 8b) we can

discover nuanced differences: *i)* because of the additives, the separate peaks characteristic of cement merge, *ii)* the contribution of more bound water types slightly increases. The changes are more pronounced when studying the amplitudes of the T_2 peaks (see in Fig. 8c) of the pore types presented above. One can observe that the added metakaolin (Mc10–30) increased the influence of the pores in the CSH gel (A_{a-b}), mainly the contribution of the smaller intra CSH layer pores. The ratio of the capillary pore decreased from 19 % to 6 % with the addition of 10–20 % metakaolin. In case of fly ash (Fc10–30) the ratio of pores in the CSH gel increased similarly to metakaolin or to a slightly greater extent, however, in this case, the amount of inter CSH gel pores is more significant. For samples with 10 % and 30 % fly ash content the contribution of capillary pores decreased to \sim 2 %.

3.3. Effect of additives on the movement and connectivity of water types in hardened cement

The 2D T_I - T_2 correlation NMR relaxometry provides information on the permeability of the pores and the exchange processes between the individual water types. [10,21,66] In contrast to 1D CPMG measurements, here the detection of the T_2 transverse relaxation process is encoded in the T_I longitudinal relaxation measurement, so both relaxation processes and their correlation are recorded. The two relaxation processes can be significantly different for chemically bound, adsorbed hydrogens, and hydrogen in water confined in small pores. For chemically bound water in the CSH gel T_I is long (> 100 ms), but T_2 is short (~0.01 ms) [21], while for water in the CSH gel pores, where the movement of the molecules is less hindered, T_I and T_2 are both short since the relaxing effect of the surface still accelerates the relaxation processes. As

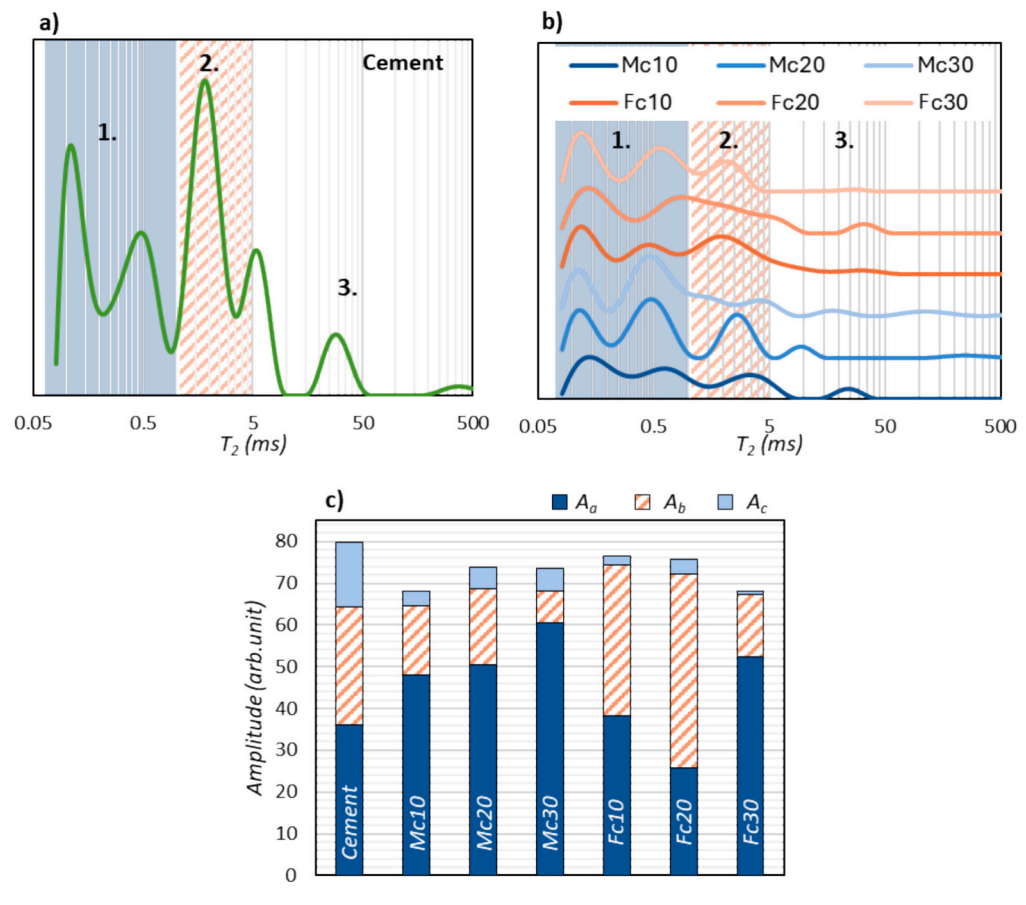


Fig. 8. T_2 relaxation time distribution in a) hardened Portland cement and b) 10–30 % metakaolin (blue) and fly ash (orange) containing cement composites with the identified pore types (1- intra CSH sheet pore, 2- inter CSH gel pore, 3- capillary pore). c) Effect of pozzolans on the amplitude of water in different pores. (For interpretation of the references to colour in this figure legend, the reader is referred to the web version of this article.)

the size of the confinements increases, the relaxing effect of the surface decreases causing longer T_1 and T_2 in the capillary pores [10,21].

The 2D T_1 - T_2 correlation maps of the composite samples of 20 % pozzolan content (Mc20 and Fc20) were compared to that of the pure Portland cement (see in Fig. 9). The water domains identified on the 1D T_2 time distributions (see in Fig. 8a-b) can be observed in the diagonal of the 2D maps: on the left the signal of the intra CSH sheet pores is present with high intensity (1); with longer relaxation times the inter CSH gel pores are visible (2), while the third low- intensity signal on the diagonal at long relaxation times can be assigned to the capillary pores (3). The 1D T_1 and T_2 distributions derived from the 2D T_1 - T_2 correlation maps are shown in Fig. SI 10. The position of the diagonal peaks is similar for pure Portland cement and Mc20, however, for Fc20 the peaks are shifted to shorter time intervals. The intensity of the signals of the CSH gel is enhanced by the addition of pozzolans corroborating the 1D distributions. This is especially observable in the case of the fly ash-containing sample, where water in the small CSH sheet pores exhibit broad T_1 distribution beside the short T_2 .

The peaks in the diagonal are slightly shifted, from the principal diagonal $T_1=T_2$ to $T_1=2$ T_2 (marked with dashed line in Fig. 9) in case of cement and Mc20, while in case of Fc20 the peaks mainly align to $T_1=4$ T_2 (marked with dotted line). Such features were also observed in cementitious samples by McDonald et al., who explained it by the different surface diffusion correlation (τ_m) and surface residence times (τ_s) of water in the materials according to the surface diffusion model of relaxation. [21,66,67] They found that the ratio of the time constants is $\tau_m/\tau_s\approx 10^{-2}$ in case of $T_1=2$ T_2 , while it is $\tau_m/\tau_s\approx 10^{-4}$ in case of $T_1=1$

4 T_2 , the reciprocal value of which (τ_s/τ_m) shows the "affinity" of the surface to the solvent [21,68]. This approach refers to a stronger interaction between the water molecules and the fly ash containing component, as τ_d and τ_l values already indicated in the case of FFC NMR measurements following the early hydration of cement (detailed in Section 3.1.2.)

The separation of the peaks indicates that each type of water is found in a different environment, meaning that the pore structure is less opened [21,69]. This can be clearly observed in the case of the metakaolin containing sample (Mc20), where the individual signals less merge compared to the other two samples. The off-diagonal cross peaks can be interpreted in two ways: if $T_1 >> T_2$ the peak can be attributed to hydrogen in solid-like environment, chemically bound in the CSH gel [21]. If the difference is not of this magnitude and the cross peak also appears in the 2D T_2 - T_2 correlation maps, then chemical exchange occurs between different pores [21,66]. Based on the conclusions of McDonald et al., the cross peaks seen in the upper left corner of the 2D T_1 - T_2 correlation maps were assigned to the chemical exchange between the CSH gel and the capillary pores [21,66,67]. The addition of the pozzolans clearly decreased the possibility of the exchange processes.

A key feature of the binders used in radioactive waste management is the extent to which they can inhibit the diffusion of water, and thus the leaching of radionuclides. The self - diffusion of water was measured in 10–30 % metakaolin and fly ash containing cement composites and was compared to the one previously measured in pure Portland cement (see in Fig. SI. 11) [22]. The self- diffusion of liquids in a porous structure is usually measured by sequences using gradient pulses (PGSE NMR),

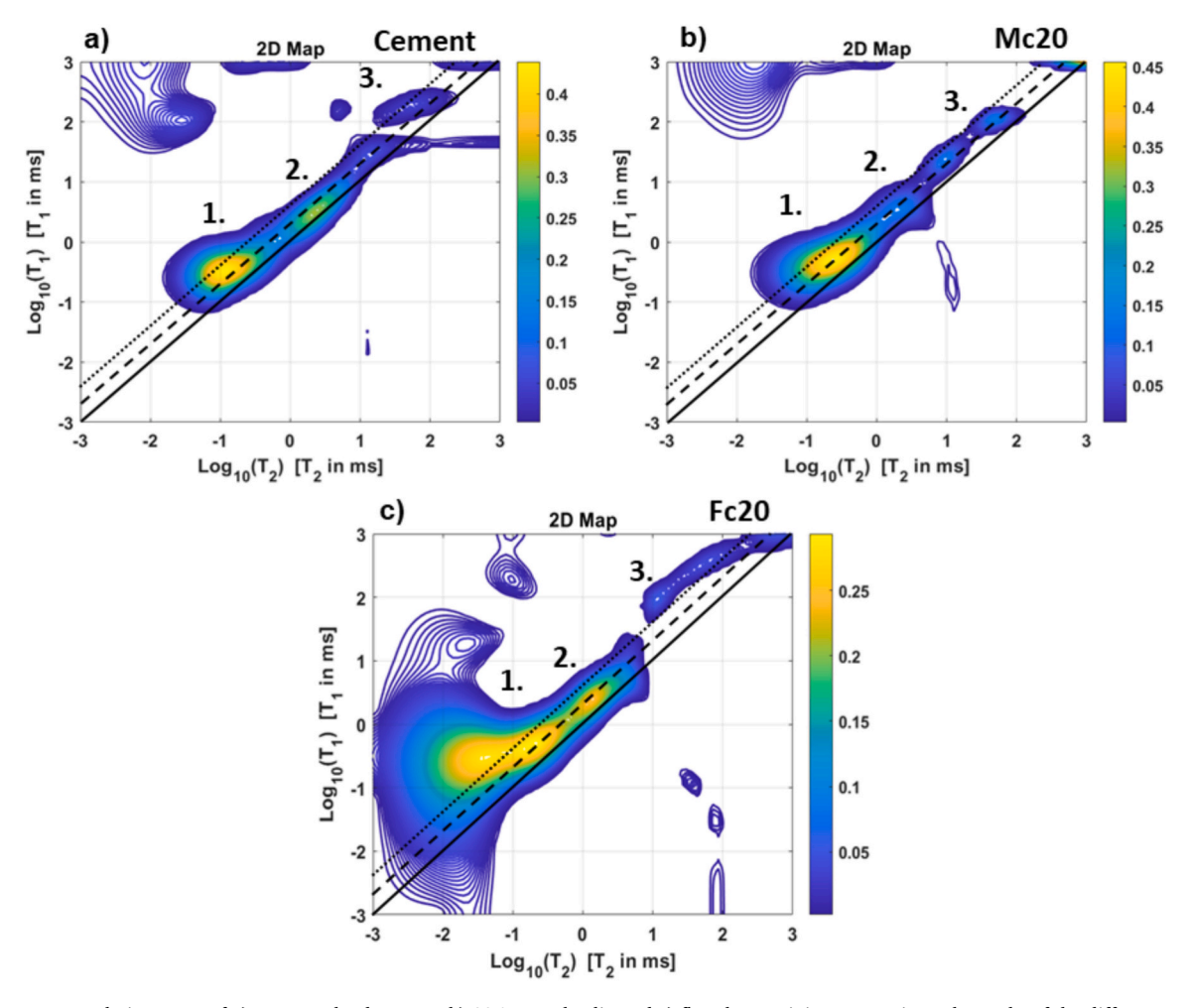


Fig. 9. The T_1 - T_2 correlation maps of a) pure Portland cement, b) 20 % metakaolin and c) fly ash containing composites. The peaks of the different pore types are marked as: 1- intra CSH sheet pore, 2- inter CSH gel pore, 3- capillary pore. The dashed ($T_1 = 2$ T_2) and dotted ($T_1 = 4$ T_2) lines show the shifted principal diagonal.

however, in the case of samples containing magnetic inhomogeneities (e.g. Fe³⁺) the T_1 and T_2 relaxation processes of confined water are significantly accelerated, therefore these sequences are not suitable for studying diffusion processes. For testing such systems, the H₂O-D₂O exchange diffusion technique can be applicable [20,22,30]. The basis of this method is that the H_2O saturated sample is placed in D_2O , and only the H_2O protons inside the cement samples are detected during the diffusion process. As the H_2O diffuses out of the cement and exchanges with D_2O , the measured proton intensity exponentially decreases over time as it is shown in Fig. 10. Comparing the exponential decays two main differences can be observed between the samples: I) the rate of the decay process and II) the residual signal intensity. The ratio of the added pozzolan affects mainly the rate of the water signal decay for metakaolin, while it influences the residual signal intensity for fly ash. In the case of the metakaolin series, the diffusion process is elongated compared to the fly ash containing samples indicating the more hindered movement of the water molecules. At low metakaolin content (Mc10), a relatively faster decay can be seen similarly to pure Portland cement (see in Fig.SI. 11). The decay becomes more prolonged by increasing the amount of added metakaolin, as more pozzolanic hydration product forms (Fig. 10a). Fly ash has less influence on the course of the curve, but rather on the intensity of the residual signal, which can be attributed to the bound, non- or very slowly diffusing water (Fig. 10b). The significant contribution of this strongly bound water type was already revealed on the 2D T_1 - T_2 correlation map of Fc20 (see in Fig. 9c). The amount of this water type increases with the fly ash content as the change of the residual signal intensities suggests. Furthermore, the observed residual signal intensities well correlate with the N₂ porosimetry data; higher intensity means more non-evaporable water in the micropores, resulting in less available pore volume for N2 gas thus in lower pore volumes and surface area.

The obtained decay curves were fitted with the mathematical model derived by J. Crank [70]. This model describes the diffusion processes in an infinite cylinder (C_{cyl}) and in a plane sheet (C_{ps}), as the product of two exponentials:

$$C^* = \frac{M(t) - M(t = \infty)}{M(t = 0) - M(t = \infty)} = C_{ps}C_{cyl}$$
(3)

$$C_{ps} = \sum\nolimits_{n=0}^{\infty} \frac{2\alpha(1+\alpha)}{1+\alpha+\alpha^2p_n^2} exp\left(-D_p p_n^2 \frac{t}{l^2}\right) \tag{4}$$

$$C_{cyl} = \sum_{n=0}^{\infty} \frac{4\alpha(1+\alpha)}{4+4\alpha+\alpha^{2}p_{z}^{2}} exp\left(-D_{p}p_{n}^{2}\frac{t}{r^{2}}\right)$$
 (5)

where C^* is the change in the concentration of light water, M is the intensity of the measured signal, α is the volume ratio of heavy to light water, p_n is the square root of the error function, D_p is the diffusion coefficient of water, t is the duration of the measurement, while t and t

are the radius and length of the cylinder, respectively [20,70]. The primary data were best fitted as a product of three exponential sums. The derived diffusion coefficients are presented in Fig. 11. They are in all cases at least one order of magnitude lower than the diffusion coefficient of bulk water ($D = 2.3 \times 10^{-9} \, \text{m}^2/\text{s}$) [71], referring to strongly restricted diffusion of water in the samples.

In the metakaolin containing samples three different diffusion coefficients were found: $D_{1,2}=1.0\times 10^{-11}$ - 7.5 \times 10⁻¹¹ m²/s, $D_3=2.2\times 10^{-12}$ –9.4 \times 10⁻¹² m²/s (detailed in Table SI 1). The slowest diffusion (D_3) process can be assigned to the restricted movement of water in the swollen CSH gel layer, while the faster diffusion $(D_{1,2})$ can take place in the larger capillary pores. Similar results were observed by Fleury et al. for pure cement [30]. We recently reported the following diffusion coefficients of water in pure Portland cement: $D_1 = 9.6 \times 10^{-10} \text{ m}^2/\text{s}, D_2 =$ $2.4 \times 10^{-10} \text{ m}^2/\text{s}$, $D_3 = 3.1 \times 10^{-12} \text{ m}^2/\text{s}$ [22]. It means, that the addition of metakaolin resulted in an order of magnitude lower value for the diffusion coefficient of water in larger capillary pores compared to pure cement. In the fly ash containing composites two diffusion coefficients described the movement of confined water: $D_1 = 1.5 \times 1.5$ 10^{-10} –3.7 × 10^{-10} m²/s, $D_2 = 2.2 \times 10^{-12}$ –5.3 × 10^{-12} m²/s (detailed in Table SI 1). Water diffuses similarly within the fly ash containing cement as in pure cement. Considering the inhibition of diffusion within the solid matrix, the addition of metakaolin in 20 % resulted in the most

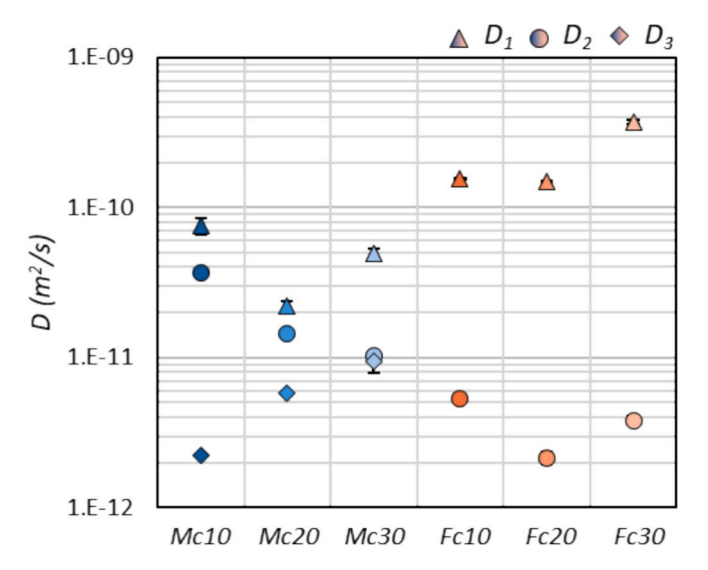


Fig. 11. The self- diffusion coefficients (D_{1-3}) of water in 10–30 % metakaolin (blue) and fly ash (orange) containing cement composites. (For interpretation of the references to colour in this figure legend, the reader is referred to the web version of this article.)

80

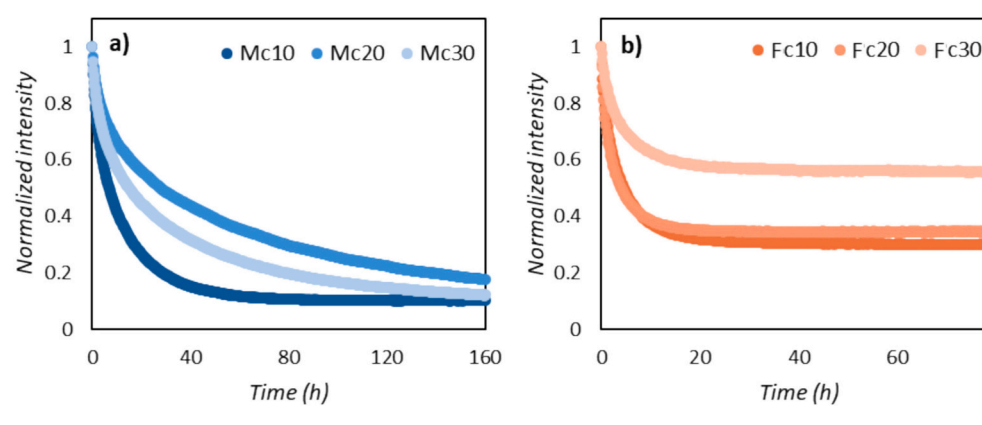


Fig. 10. The normalized intensity of the proton signal over time in 10-30 % a) metakaolin and b) fly ash containing cement composites.

promising composition.

4. Conclusions

This study describes the impact of metakaolin and fly ash on the early hydration and the formed pore structure of Portland cement in details using various techniques. The early hydration of pozzolan containing cement composite samples was followed by low-field NMR relaxometry and FFC- NMR. The two additives exerted their pozzolanic effects at different stages of the cement hydration. Metakaolin, due to its higher active aluminate and silicate content, enhanced the rate of the deceleration period (IV) compared to pure cement. In contrast, fly ash acted as a filler material, slowed down the precipitation of hydration products, thus affecting the entire hydration process by extending the induction period and decreasing the rate of the acceleration and deceleration periods. This study is the first to apply the 3-Tau model for analyzing the FFC- NMR dispersion curves to investigate the effect of pozzolan additives during the early hydration of cement. The derived parameters revealed that the interaction between the solid surface and the water molecules is the strongest in the case of the fly ash containing composites (Fc), and the available space for the precipitation is the lowest for these samples through the early hydration.

At the end of the 28-day hydration process, the porous structure of the hardened composites was characterized by scanning electron microscopy and N₂ porosimetry in dry state on the micro- and nanoscale, respectively. The metakaolin containing (Mc) samples possess a more contiguous solid matrix with few macroscopic voids, where the microand mesopores dominated the porous structure. In contrast, in the fly ash composites, the added fly ash particles increased the structural heterogeneity and enhanced the contribution of the macropores alongside micropores in the sample. The dominance of the small intra CSH layer and inter CSH gel pores in the pozzolan containing composites was also observable in the T_2 relaxation time distributions of the wet samples. The 2D T_1 - T_2 correlation measurements more effectively highlighted the structural differences between the samples: a significant amount of bound water and a strong interaction between the solid surface and the water molecules in the fly ash containing samples can be revealed, consistent with the FFC- NMR results, while in the metakaolin composites a less permeable structure can be observed. The structural differences were reflected by the diffusion coefficients of the confined water. Water diffused slower in the capillary pores of the Mc samples and the 20 % metakaolin content resulted in the least permeable matrix. In the fly ash composites, diffusion of water is fast from the macropores, however, a significant amount of bound water is retained in the micropores, being in connection with the available pore volume for N₂ gas.

Overall, a similarity between cement and Mc samples was observed, while Fc samples showed significant change in some properties, which can be explained with their dissimilar pozzolanic activities. Metakaolin exerts its pozzolanic effect on cement hydration earlier than fly ash, simultaneously to the C₃S cement phase. This results in a similar pore structure for pure cement and the metakaolin composites, however, the addition of metakaolin increases the contribution of the pores in the CSH gel, resulting in decreased water mobility within the hardened sample. In contrast to this, in the Fc composites the growth of hydrates inside the refining pores may be more restrained, and this lower pozzolanic activity (filler effect and less available space) results in the formation of a pore structure with high micro- and macroporosity. Regarding the aimed application, metakaolin additive leads to a less permeable, more homogenous and contiguous solid matrix, while fly ash composites retain high amount of water in the micropores, which both properties can be advantageous for the long-term safe disposal of radioactive waste.

CRediT authorship contribution statement

Vanda Papp: Writing - original draft, Visualization, Investigation,

Data curation. **Ioan Ardelean:** Methodology, Investigation. **Anna Bulátkó:** Investigation. **Krisztina László:** Writing – original draft, Methodology, Data curation. **Attila Csík:** Writing – original draft, Visualization, Investigation. **Róbert Janovics:** Funding acquisition, Conceptualization. **Mónika Kéri:** Writing – review & editing, Supervision, Conceptualization.

Declaration of competing interest

The authors declare that they have no known competing financial interests or personal relationships that could have appeared to influence the work reported in this paper.

Acknowledgement

The research was supported by the National Research, Development and Innovation Office – NKFIH [PD 135169, K 131989]. Project no. C1762343 [RH/322-2/2022] has been implemented with the support provided by the Ministry of Culture and Innovation of Hungary from the National Research, Development and Innovation Fund, financed under the KDP-2021 funding scheme.

The research was also supported by the University of Debrecen Scientific Research Bridging Fund (DETKA) and by the University of Debrecen Program for Scientific Publication. Furthermore, M.K. is grateful for the support from the János Bolyai Research Scholarship of the Hungarian Academy of Sciences. The research is part of project no. BME-NVA-02, implemented with the support of the Ministry of Innovation and Technology of Hungary from the National Research, Development and Innovation Fund, and financed under the TKP2021 funding scheme. We are grateful to István Bányai and Mihai Marius Rusu for the useful discussions and suggestions.

Appendix A. Supplementary data

Supplementary data to this article can be found online at https://doi.org/10.1016/j.cemconres.2025.107928.

Data availability

Data will be made available on request.

References

- S. Barbhuiya, B.B. Das, T. Qureshi, D. Adak, Cement-based solidification of nuclear waste: mechanisms, formulations and regulatory considerations, J. Environ. Manag. 356 (2024) 120712.
- [2] J. Kofátková, J. Zatloukal, P. Reiterman, K. Kolář, Concrete and cement composites used for radioactive waste deposition, J. Environ. Radioact. 178-179 (2017) 147–155.
- [3] J. Li, L. Chen, J. Wang, Solidification of radioactive wastes by cement-based materials, Prog. Nucl. Energy 141 (2021) 103957.
- [4] D. Marchon, R.J. Flatt, 8 mechanisms of cement hydration, in: P.-C. Aïtcin, R. J. Flatt (Eds.), Science and technology of concrete admixtures, Woodhead Publishing, 2016, pp. 129–145.
- [5] M. Ochs, D. Mallants, L. Wang, Cementitious materials and their sorption properties, in: M. Ochs, D. Mallants, L. Wang (Eds.), Radionuclide and metal sorption on cement and concrete, Springer International Publishing, Cham, 2016, pp. 5-16.
- [6] R.F. Feldman, P.J. Sereda, A model for hydrated Portland cement paste as deduced from sorption-length change and mechanical properties, Mater. Constr. 1 (6) (1968) 509–520.
- [7] H.M. Jennings, Refinements to colloid model of C-S-H in cement: CM-II, Cem. Concr. Res. 38 (3) (2008) 275–289.
- [8] C. Badea, A. Pop, C. Mattea, S. Stapf, I. Ardelean, The effect of curing temperature on early hydration of gray cement via fast field cycling-NMR Relaxometry, Appl. Magn. Reson. 45 (12) (2014) 1299–1309.
- [9] A. Bede, A. Scurtu, I. Ardelean, NMR relaxation of molecules confined inside the cement paste pores under partially saturated conditions, Cem. Concr. Res. 89 (2016) 56–62.
- [10] C. Cadar, A. Cretu, M. Moldovan, C. Mattea, S. Stapf, I. Ardelean, NMR T1–T2 correlation analysis of molecular absorption inside a hardened cement paste containing silanised silica fume, Mol. Phys. 117 (7–8) (2019) 1000–1005.

- [11] M.M. Rusu, D. Faux, I. Ardelean, Monitoring the effect of calcium nitrate on the induction period of cement hydration via low-field NMR Relaxometry, Molecules 28 (2) (2023) 476.
- [12] P.J. McDonald, V. Rodin, A. Valori, Characterisation of intra- and inter-C-S-H gel pore water in white cement based on an analysis of NMR signal amplitudes as a function of water content, Cem. Concr. Res. 40 (12) (2010) 1656–1663.
- [13] J.P. Korb, L. Monteilhet, P.J. McDonald, J. Mitchell, Microstructure and texture of hydrated cement-based materials: a proton field cycling relaxometry approach, Cem. Concr. Res. 37 (3) (2007) 295–302.
- [14] I. Medved', R. Černý, Modeling of radionuclide transport in porous media: a review of recent studies, J. Nucl. Mater. 526 (2019) 151765.
- [15] A.B. Degefa, H. Yoon, S. Park, H. Yoon, J. Bak, S. Park, Machine learning applied to predicting phase assemblages of hardened cementitious systems, Ceram. Int. 50 (10) (2024) 17783–17795.
- [16] M. Frías, M.I.S. de Rojas, J. Cabrera, The effect that the pozzolanic reaction of metakaolin has on the heat evolution in metakaolin-cement mortars, Cem. Concr. Res. 30 (2) (2000) 209–216.
- [17] F. Moghaddam, V. Sirivivatnanon, K. Vessalas, The effect of fly ash fineness on heat of hydration, microstructure, flow and compressive strength of blended cement pastes, Case Stud. Construct. Mater. 10 (2019) e00218.
- [18] N. Saboo, S. Shivhare, K.K. Kori, A.K. Chandrappa, Effect of fly ash and metakaolin on pervious concrete properties, Constr. Build. Mater. 223 (2019) 322–328.
- [19] R. Snellings, P. Suraneni, J. Skibsted, Future and emerging supplementary cementitious materials, Cem. Concr. Res. 171 (2023) 107199.
- [20] M. Fleury, G. Berthe, T. Chevalier, Diffusion of water in industrial cement and concrete, Magn. Reson. Imaging 56 (2019) 32–36.
- [21] P.J. McDonald, J.P. Korb, J. Mitchell, L. Monteilhet, Surface relaxation and chemical exchange in hydrating cement pastes: a two-dimensional NMR relaxation study, Phys. Rev. E 72 (1) (2005) 011409.
- [22] V. Papp, R. Janovics, T. Péter Kertész, Z. Nemes, T. Fodor, I. Bányai, M. Kéri, State and role of water confined in cement and composites modified with metakaolin and additives, J. Mol. Liq. 388 (2023) 122716.
- [23] A. She, W. Yao, Probing the hydration of composite cement pastes containing fly ash and silica fume by proton NMR spin-lattice relaxation, SCIENCE CHINA Technol. Sci. 53 (6) (2010) 1471–1476.
- [24] D.D. Lasic, J.M. Corbett, J. Jian, J.C. MacTavish, M.M. Pintar, R. Blinc, G. Lahajnar, NMR spin grouping in hydrating cement at 200 MHz, Cem. Concr. Res. 18 (4) (1988) 649–653.
- [25] L. Miljkovic, D. Lasic, J.C. MacTavish, M.M. Pintar, R. Blinc, G. Lahajnar, NMR studies of hydrating cement: a spin-spin relaxation study of the early hydration stage, Cem. Concr. Res. 18 (6) (1988) 951–956.
- [26] Y.-J. Tang, Z.-Q. Shan, G.-J. Yin, L. Miao, S.-S. Wang, Z.-Y. Zhang, Low-field nuclear magnetic resonance investigation on early hydration characterization of cement paste mixed with mineral admixtures. Buildings 13 (9) (2023) 2318.
- [27] B. Walkley, J.L. Provis, Solid-state nuclear magnetic resonance spectroscopy of cements, Mater. Today Adv. 1 (2019) 100007.
- [28] A. Pop, C. Badea, I. Ardelean, The effects of different superplasticizers and water-to-cement ratios on the hydration of gray cement using T2-NMR, Appl. Magn. Reson. 44 (10) (2013) 1223–1234.
- [29] P.F. Faure, S. Rodts, Proton NMR relaxation as a probe for setting cement pastes, Magn. Reson. Imaging 26 (8) (2008) 1183–1196.
- [30] M. Fleury, T. Chevalier, G. Berthe, W. Dridi, M. Adadji, Water diffusion measurements in cement paste, mortar and concrete using a fast NMR based technique, Constr. Build. Mater. 259 (2020) 119843.
- [31] Handling and processing of radioactive waste from nuclear applications, International Atomic Energy Agency, Vienna, 2001.
- [32] O.M. Jensen, P.F. Hansen, Water-entrained cement-based materials: I. Principles and theoretical background, Cem. Concr. Res. 31 (4) (2001) 647–654.
- [33] S. Brunauer, P.H. Emmett, E. Teller, Adsorption of gases in multimolecular layers, J. Am. Chem. Soc. 60 (2) (1938) 309–319.
- [34] M. Dubinin, In the equation of the characteristic curve of activated charcoal, Dokl. Akad. Nauk SSSR (1947) 327–329.
- [35] E.P. Barrett, L.G. Joyner, P.P. Halenda, The determination of pore volume and area distributions in porous substances. I. Computations from nitrogen isotherms, J. Am. Chem. Soc. 73 (1) (1951) 373–380.
- [36] S. Meiboom, D. Gill, Modified spin-Echo method for measuring nuclear relaxation times, Rev. Sci. Instrum. 29 (8) (1958) 688–691.
- [37] Does, M. D.; Juttukonda, M. R.; Dortch, R. D. MERA Toolbox (1D,2D Multiexponential Relaxation Analysis), 2.02 Vanderbilt University.
- [38] V. Bortolotti, R.J.S. Brown, P. Fantazzini, G. Landi, F. Zama, I2DUPEN: improved 2DUPEN algorithm for inversion of two-dimensional NMR data, Microporous Mesoporous Mater. 269 (2018) 195–198.
- [39] S. Muncaci, C. Mattea, S. Stapf, I. Ardelean, Frequency-dependent NMR relaxation of liquids confined inside porous media containing an increased amount of magnetic impurities, Magn. Reson. Chem. 51 (2) (2013) 123–128.
- [40] R. Kogon, D. Faux, 3TM: software for the 3-tau model, SoftwareX 17 (2022)
- [41] P.C. Aïtcin, 3 Portland cement, in: P.-C. Aïtcin, R.J. Flatt (Eds.), Science and technology of concrete admixtures, Woodhead Publishing, 2016, pp. 27–51.

- [42] P. Barrie, Characterization of porous media using NMR methods 41 (2000) 265–316.
- [43] S. Jurt, O. Zerbe, Applied NMR spectroscopy for chemists and life scientists, Wiley-VCH Verlag GmbH, 2013.
- [44] L. Liu, Z. He, X. Cai, S. Fu, Application of low-field NMR to the pore structure of concrete, Appl. Magn. Reson. 52 (1) (2021) 15–31.
- [45] S. Rahimi-Aghdam, Z.P. Bažant, M.J. Abdolhosseini Qomi, Cement hydration from hours to centuries controlled by diffusion through barrier shells of C-S-H, J. Mech. Phys. Solids 99 (2017) 211–224.
- [46] E. John, B. Lothenbach, Cement hydration mechanisms through time a review, J. Mater. Sci. 58 (24) (2023) 9805–9833.
- [47] B. Lothenbach, K. Scrivener, R.D. Hooton, Supplementary cementitious materials, Cem. Concr. Res. 41 (12) (2011) 1244–1256.
- [48] Marchon, D.; Flatt, R. J. 12 impact of chemical admixtures on cement hydration. Science and technology of concrete admixtures, Aitcin, P.-C.; Flatt, R. J., Eds. Woodhead Publishing: 2016; pp. 279–304.
- [49] Mardani-Aghabaglou, A.; İnanSezer, G.; Ramyar, K., Comparison of fly ash, silica fume and metakaolin from mechanical properties and durability performance of mortar mixtures viewpoint. Constr. Build. Mater. 2014, 70, 17-25.
- [50] J. Skibsted, R. Snellings, Reactivity of supplementary cementitious materials (SCMs) in cement blends, Cem. Concr. Res. 124 (2019) 105799.
- [51] H. Liu, Z. Sun, J. Yang, Y. Ji, A novel method for semi-quantitative analysis of hydration degree of cement by 1H low-field NMR, Cem. Concr. Res. 141 (2021) 106329.
- [52] P.C. Aïtcin, 4 supplementary cementitious materials and blended cements, in: P.-C. Aïtcin, R.J. Flatt (Eds.), Science and technology of concrete admixtures, Woodhead Publishing, 2016, pp. 53–73.
- [53] F. Lagier, K.E. Kurtis, Influence of Portland cement composition on early age reactions with metakaolin, Cem. Concr. Res. 37 (10) (2007) 1411–1417.
- [54] J.M. Justice, K.E. Kurtis, Influence of Metakaolin surface area on properties of cement-based materials, J. Mater. Civ. Eng. 19 (9) (2007) 762–771.
- [55] J.P. Korb, NMR and nuclear spin relaxation of cement and concrete materials, Curr. Opin. Colloid Interface Sci. 14 (3) (2009) 192–202.
- [56] C. Badea, A. Bede, I. Ardelean, The effect of silica fume on early hydration of white Portland cement via fast field cycling-NMR relaxometry, AIP Conf. Proc. 1917 (1) (2017).
- [57] D. Faux, R. Kogon, V. Bortolotti, P. McDonald, Advances in the interpretation of frequency-dependent nuclear magnetic resonance measurements from porous material, Molecules 24 (20) (2019) 3688.
- [58] D.A. Faux, P.J. McDonald, A model for the interpretation of nuclear magnetic resonance spin-lattice dispersion measurements on mortar, plaster paste, synthetic clay and oil-bearing shale, Microporous Mesoporous Mater. 269 (2018) 39–42.
- [59] K.L. Scrivener, A. Nonat, Hydration of cementitious materials, present and future, Cem. Concr. Res. 41 (7) (2011) 651–665.
- [60] Matsushima, T. Desorption kinetics ★. Encyclopedia of interfacial chemistry, Wandelt, K., Ed. Elsevier: Oxford, 2018; pp. 59–63.
- [61] P. Chindaprasirt, C. Jaturapitakkul, T. Sinsiri, Effect of fly ash fineness on microstructure of blended cement paste, Constr. Build. Mater. 21 (7) (2007) 1534–1541.
- [62] M. Thommes, K. Kaneko, A.V. Neimark, J.P. Olivier, F. Rodriguez-Reinoso, J. Rouquerol, K.S.W. Sing, Physisorption of gases, with special reference to the evaluation of surface area and pore size distribution (IUPAC technical report), Pure Appl. Chem. 87 (9–10) (2015) 1051–1069.
- [63] Y. Song, J.-w. Zhou, Z.-n. Bian, G.-z. Dai, Pore structure characterization of hardened cement paste by multiple methods, Adv. Mater. Sci. Eng. 2019 (1) (2019) 3726953
- [64] I. Odler, The BET-specific surface area of hydrated Portland cement and related materials, Cem. Concr. Res. 33 (12) (2003) 2049–2056.
- [65] A. Korpa, R. Trettin, The influence of different drying methods on cement paste microstructures as reflected by gas adsorption: comparison between freeze-drying (F-drying), D-drying, P-drying and oven-drying methods, Cem. Concr. Res. 36 (4) (2006) 634–649.
- [66] P.J. McDonald, J. Mitchell, M. Mulheron, L. Monteilhet, J.-P. Korb, Twodimensional correlation relaxation studies of cement pastes, Magn. Reson. Imaging 25 (4) (2007) 470–473.
- [67] P.J. McDonald, J. Mitchell, M. Mulheron, P.S. Aptaker, J.-P. Korb, L. Monteilhet, Two-dimensional correlation relaxometry studies of cement pastes performed using a new one-sided NMR magnet, Cem. Concr. Res. 37 (3) (2007) 303–309.
- [68] S. Godefroy, J.P. Korb, M. Fleury, R.G. Bryant, Surface nuclear magnetic relaxation and dynamics of water and oil in macroporous media, Phys. Rev. E 64 (2) (2001) 021605.
- [69] Y.Q. Song, L. Venkataramanan, M.D. Hürlimann, M. Flaum, P. Frulla, C. Straley, T1–T2 correlation spectra obtained using a fast two-dimensional Laplace inversion, J. Magn. Reson. 154 (2) (2002) 261–268.
- [70] J. Crank, The mathematics of diffusion, Oxford university press, 1979.
- [71] R. Mills, Self-diffusion in normal and heavy water in the range 1-45.Deg, J. Phys. Chem. 77 (5) (1973) 685–688.